Electrochemical oxidation of Naproxen in aqueous matrices: Elucidating the intermediates' eco-toxicity, by assessing its degradation pathways via experimental and density functional theory (DFT) approaches

Ling Feng, Weiwei Song, Nihal Oturan, Minoo Karbasi, Eric D van Hullebusch, Giovanni Esposito, Stefanos Giannakis, Mehmet A Oturan

Electrochemical oxidation of Naproxen in aqueous matrices: Elucidating the intermediates' eco-toxicity, by assessing its degradation pathways via experimental and Density Functional Theory (DFT) approaches

Ling Feng[1], Weiwei Song[1], Nihal Oturan[2], Minoo Karbasi[3], Eric D. van Hullebusch[4], Giovanni Esposito[5], Stefanos Giannakis[6*], Mehmet A. Oturan[2*]

[1] School of Ecology and Environment, Inner Mongolia University, University W. Road, 010021, Huhhot, Inner Mongolia (P.R.), China

[2] Université Gustave Eiffel, Laboratoire Géomatériaux et Environnement, EA 4508, 77454 Marne-la-Vallée, Cedex 2, France

[3] Department of Materials Engineering, Bu-Ali Sina University, Hamedan 65178-38695, Iran

[4] Institut de Physique Du Globe de Paris, Université de Paris, CNRS, F-75005, Paris, France

[5] Department of Civil, Architectural and Environmental Engineering, University of Napoli "Federico II", Via Claudio 21, 80125 Napoli, Italy

[6] Universidad Politécnica de Madrid, E.T.S. de Ingenieros de Caminos, Canales y Puertos, Departamento de Ingeniería Civil: Hidráulica, Energía y Medio Ambiente, Unidad docente Ingeniería Sanitaria, c/ Profesor Aranguren, s/n, ES-28040 Madrid, Spain

**** Corresponding Author: Dr. Stefanos Giannakis, E-mail:*** stefanos.giannakis@upm.es

**** Corresponding Author: Prof. Dr. Mehmet A. Oturan, E-mail:*** mehmet.oturan@univ-eiffel.fr

Full text published in: Chemical Engineering Journal

Permanent Address: https://doi.org/10.1016/j.cej.2022.138483

Abstract

The removal of the non-steroidal anti-inflammatory drug (NSAID) Naproxen (NAX) in water by hydroxyl radicals (•OH) was performed by electrochemical advanced oxidation processes either with Pt or BDD anodes and a 3D carbon felt cathode. The degradation of NAX by (•OH vs. electrolysis time) was well fitted to a pseudo-first-order reaction rate kinetic. The detected reaction intermediates (aromatic compounds and carboxylic acids) were experimentally monitored during the process via LC, while density functional theory (DFT) was applied to uncover undetected intermediates, some for the first time in literature. The formation of toxic intermediates with higher toxicity than NAX were identified, such as IMS4b (6-Methoxy-1-[1-(6-methoxynaphthalen-2-yl) ethyl] naphthalen-2-ol), catechol, and glycolic acid. Based on these data, a detailed oxidation pathway of NAX by •OH was proposed. The evolution of solution toxicity indicated that formed toxic intermediates were subsequently removed during the TOC removal process. Finally, almost complete mineralization of NAX was achieved in simulated urine or wastewater, by the electro-Fenton treatment with an optimized dose of iron as catalyst, showing the EAOPs' potential to efficiently remove NAX even from challenging matrices. In extension, the strategies developed can be applied to the treatment of other NSAIDs.

Keywords: Naproxen, Electro-Fenton, Reaction intermediates, Mineralization pathway, Density functional theory, Toxicity

1. Introduction

The global pharmaceutical market has experienced a significant growth over the recent decades, with thousands of tons of pharmaceuticals consumed worldwide [1]. Among these pharmaceuticals, non-steroidal anti-inflammatory (NSAIDs) are used by more than 30 million people every day. Naproxen (NAX 6-methoxy-α-methyl-2-naphthalene acetic acid) is found in the list of popular pharmaceuticals consumption (Table S1). It was monitored in environmental samples globally as frequently as Diclofenac [2], at concentrations in waters from ten to five hundred-fold greater than the threshold value suggested by the European Medicine Agency (EMEA) [3].

Nearly 60% of NAX is excreted as metabolites and 10% as unchanged form leave our bodies via urine. Researchers have considered NAX to be an emerging contaminant, considering its trace levels in the bile of fish of lakes receiving treated wastewater from municipal WWTPs [4]. Several works have proved that long-term exposure of NAX can increase the potential of heart attack in humans [5, 6]. Furthermore, the by-products of NAX pose a chronic toxicity higher than its acute toxicity levels by bioassay tests, which may be due to the stability of the NAX chemical structure (i.e., the naphthalene ring) [4, 7, 8].

It is accepted that the effluents (96% of occurrence) play an important role as pollutant sources to surface water [9]. Unfortunately, the pharmaceutical compounds and their metabolites, usually treated by WWTPs, reach the environment without undergoing any changes [10], since conventional treatment methods are unable to remove them. Even more, their ecotoxicity, as well as their metabolites or mixture of compounds, are still poorly investigated, raising public concern on their potential risk for the organisms living in terrestrial and aquatic environments [2, 11, 12]. The physicochemical properties of NAX limit its biodegradation by traditional wastewater treatment

processes leads to appeal for more effective treatment methods such as the advanced oxidation processes (AOPs) [13].

A variety of advanced oxidation processes, including UV photolysis of chemical oxidants (e.g., H_2O_2, chlorine, peracetic acid, etc.) [14-16], semiconductor photocatalysis, Fenton, photo Fenton and electro-Fenton have been described [15, 17-19]. Despite the high degradation of recalcitrant contaminants of these AOPs, each method has its own drawbacks; the UV light penetration maybe obstructed by water turbidity, chlorine oxidation may induce higher toxic by-products, new pollutants released into environment, high cost of storage of reagents (e.g., H_2O_2) or extra iron sludge generated as Fenton reactions [20, 21]. Electro-Fenton (EF) process has been developed as electrochemical advanced oxidation process (EAOP) where the reaction between electrogenerated the H_2O_2 from dissolved O_2 on a carbonaceous cathode and externally added catalyst (iron II salt) leads to the in-situ generation of strong oxidants hydroxyl radical ($^{\bullet}OH$) via the Fenton's reaction [22, 23]. Anodic oxidation (AO) process is another EAOP where $^{\bullet}OH$ are produced at the surface of anode [24]. $^{\bullet}OH$ is able to oxidize the organic pollutants in a non-selective oxidation way, causing, among others, ring opening and other significant transformations in a short timescale. Moreover, EF reacts till conversion of organics to final products of H_2O, CO_2 and inorganic ions [25]. Due to the potential safety risks in storage and transportation of H_2O_2, and presence of wasting reactions decreasing process efficiency, EAOPs are considered as more environmentally friendly technologies for the removal of persistent organic pollutants [26]. The main benefit is the significantly lower input of catalyst in EF, due to the regeneration of Fe^{2+} from electroreduction of Fe^{3+} at the cathode, or generation of $^{\bullet}OH$ in AO without adding any chemicals, conducting to the effective elimination of refractory organics.

In EAOPs, in situ generated $^{\bullet}OH$ react with organic compounds at a high rate, of around 10^{6-9} M^{-1} s^{-1}

[26]. However, the lifetime of important “transition” pollutants’ intermediates of pollutants is less than 10^{-2} s, rendering their detection challenging. Besides, the detailed mechanisms of degradation, specifically, to locate the •OH attack sites of the target molecules, are still not available by current analytical technologies. In this case, quantum chemical studies are applied to predict the kinetic behaviours of organic compounds in advanced oxidation technologies [27]. Recently, the by-products in the first step of the oxidation reaction between NAX and •OH in water were modeled on molecular level using a density functional theory (DFT) approach [28]. Initially, it was proposed that decarboxylation of NAX was performed by deprotonation [29], and most DFT investigations on the intermediates’ oxidation by •OH were attributed at the “side-chain” reaction of NAX [30]. However, significantly less work has been dedicated on the “ring-opening” reaction, hence important parts of the mechanism of NAX degradation mechanism by •OH oxidation systems are missing. At the same time, deep investigations of the contribution of these intermediates to the toxicity evolution during •OH-mediated oxidation of NAX are also missing.

Therefore, in our work, the main focus was the experimental and theoretical investigation on the degradation of NAX and the intermediates produced during its electrochemical advanced oxidation, and its toxicity evolution. To this end, we monitored the evolution of the toxicity of intermediates produced during processes by Microtox, while following the decay kinetics and mineralization of NAX, as well as the generated carboxylic acids. In this novel approach, our methods aimed at clarifying the dominant mechanism of NAX mineralization by identifying the most important intermediates, assessing the safety of the NAX oxidized by •OH, and allowing to set up a valid intermediates-toxicity correlation. Based on the experimentally determined by-products and theoretically obtained ones (DFT calculation results), we proposed a plausible reaction sequence for NAX degradation. Finally,

based on the present understanding on the EAOPs effect on NAX elimination, our treatment methods were assessed in a more complex matrix of high relevance to NAX, such as urine and wastewater, validating the high efficiency of these technologies in a more realistic setting.

2. Materials and methods

2.1 Chemicals and Reagents

Naproxen (NAX), sodium sulfate (Na_2SO_4) and iron (II) sulphate heptahydrate ($FeSO_4{\cdot}7H_2O$) were purchased from Sigma-Aldrich. *p*-hydroxybenzoic acid (*p*-HBA, $C_7H_6O_3$) was used as competition substrate in the kinetic experiments. NAX solution was prepared in tap water (4.56 mg/250 mL corresponding to the final concentration of 0.198 mM). The pH of the solutions was adjusted using analytical grade sulfuric acid and/or sodium hydroxide. The main intermediates and short chain carboxylic acids were all obtained from Alfa Aesar Co, whose detailed information were listed in Table SI2. For synthetic wastewaters preparation, urea (CH_4N_2O), sodium acetate ($NaC_2H_3O_2$), sodium dihydrogen phosphate (NaH_2PO_4), potassium dihydrogen phosphate (KH_2PO_4), potassium chloride (KCl), sodium hydroxide (NaOH), magnesium chloride hexahydrate ($MgCl_2{\cdot}6H_2O$), calcium chloride dihydrate ($CaCl_2{\cdot}2H_2O$) and ammonium chloride (NH_4Cl) were purchased from Merck. All other materials were purchased with purity higher than 99%.

2.2 Electrolytic experiments

Experiments were performed at room temperature (23 ± 2℃), controlled by water flow in an open, cylindrical and one-compartment cell of inner diameter of 7.5 cm, with a working volume of 250 mL. A 3D carbon-felt (18.00 cm × 6.00 cm × 0.60 cm, from Carbone-Lorraine, France) was placed on the inner wall of the electrochemical as cathode. Pt (4.5 cm^2 Pt cylindrical mesh) or boron-doped diamond (BDD) thin-film on niobium substrate (24 cm^2 from Condias, Germany) were used as anode. Anodes were placed in the center of the cell. 1 L min^{-1} of compressed air bubbled through the solution to saturate it in O_2 and the reaction medium was agitated continuously by a magnetic stirrer (800 rpm)

to ensure mass transfer during the experimental process. An AMEL 2055 potentiostat/galvanostat was used to apply a constant current. Electrolysis was conducted in 50 mM Na_2SO_4 solution as supporting electrolyte (Fig. S1). The pH of the medium was adjusted to 3 by H_2SO_4 with a CyberScan pH 1500 meter. An adequate dose of $FeSO_4 \cdot 7H_2O$ was added into initial solutions as catalyst for EF process. The experiments were conducted in triplicate in tap water, simulated urine and hospital wastewater (Table 1).

Table 1. Composition of the simulated urine and hospital wastewater.

Artificial urine	**Cl^- (NaCl)**	**Urea**	**sodium acetate**	**Na_2SO_4**	**NaH_2PO_4**	**NaOH**	**pH**
Value (mg L^{-1})	6254	16000	10250	2300	2900	120	6.1
Synthetic wastewater	**Cl^- (NaCl)**	**Urea**	**Peptone**	**Meat extract**	**$MgSO_4$**	**K_2HPO_4**	**pH**
Value (mg L^{-1})	10	30	160	110	4	28	8.0

2.3 Apparatus and analytical procedures

Concentration of NAX and its aromatic intermediates were monitored by high performance liquid chromatography (HPLC). The experiments were conducted at a lower current intensity of 50 mA, which allows slow reactions to proceed and ease the monitoring of the by-products produced during the degradation. The mobile phase for analyses was a mixture of methanol/water/acetic acid (69:29:2 (v/v/v)) at a flow rate of 0.20 mL min^{-1}. Measurements were carried out by a Merck/Hitachi LaChrom chromatograph equipped with a Purospher RP-18 column (5 μm, 25 cm×3 mm (i.d.)), coupled with

an L-2400 UV detector set at 240 nm and 40°C. The identification and quantification of carboxylic acids as terminal by-products were performed by ion-exclusion HPLC with a Supelcogel H column (4.60 mm × 25.00 cm) using a mobile phase formed of 1% H_3PO_4 solution at the detection wavelength set at 210 nm. The identification and quantification of by-products were achieved by comparison of retention time and area of peaks with that of pure products. The injection volume was 20 µL. Measurements were controlled through EZChrom Elite 3.1 software. The mineralization degree of samples was determined on a Shimadzu VCSH TOC analyzer by determining the abatement of total organic content. Reproducible total organic content (TOC) values with ±2% accuracy were obtained using the non-purgeable organic carbon (NPOC) method.

The mineralization current efficiency (MCE in %) is an indicator for assessment of the capacity of current intensity application. It can be calculated according to the Eq. (1) at a given electrolysis time t (h) [26, 31]:

$$MCE = \frac{n\,F\,Vs\,\Delta(TOC)exp}{4.32 \times 10^{7} m\,I\,t} \times 100 \qquad (1)$$

where n is the number of electrons consumed per molecule mineralized (i.e. 64), *F* is the Faraday constant (96487 C mol^{-1}), V_s is the solution volume (L), $\Delta(TOC)_{exp}$ is the experimental TOC decay (mg L^{-1}), 4.32×10^7 is a homogenization factor (3600 s h^{-1} × 12,000 mg mol^{-1}), m is the number of carbon atoms of NAX (14) and *I* is the applied current intensity (0.10 - 0.75 A).

The assessment of the potential toxicity of NAX and its intermediates was conducted following the international standard process (DIN 11348-3), by the inhibition of the luminescence (%) of bioluminescent marine bacteria *V. fischeri* (Lumistox LCK 487, Hach Lange France SAS), known as the Microtox® method. The value of the inhibition of the luminescence (%) was measured after 15 min of exposure of bacteria to treated solutions at 15 °C. The bioluminescence measurements were

performed on solutions electrolyzed at different constant current intensities (I= 0.10 and 0.30 A). The inhibition toxicity of the samples was expressed as a percentage inhibition compared to the blank (C_0 = 0 mg L^{-1} of NAX).

2.4 Computational methods

The optimized theoretical calculations were implemented using the Gaussian 16-A03-AVX2 (09 D.01 program) package based on density functional theory (DFT) [32]. Molecular geometries of all intermediates and transition states (TS) were optimized by M05-2X/6-31+G** level of theory (Fig. S2) [28]. The single point energy was calculated by B2PLYPD3 functional and def2TZVP basis set with higher accuracy. The energy calculations of all structures were thermodynamically corrected [33, 34]. The solvent effects were taken into consideration by using the solvation model of density (SMD) [35]. Vibrational analysis was carried out to confirm that each structure is a true minimum or a saddle point. Intrinsic reaction coordinate (IRC) calculations were performed to assure the transition states connected the reactants and products for each elementary reaction [36].

Conventional TS theory was used to predict the rate of reaction between molecular and •OH at 298 K in water with the standard state [37] through Eqs .2 and 3:

$$k = \sigma\Gamma(\mathrm{T})\frac{k_B T}{h}e^{-(\triangle_+^{\ddagger}G)/RT} \quad (2)$$

$$\Gamma(\mathrm{T}) = 1 + (\frac{1}{24})\left[1.44\frac{vi}{T}\right]^2 \quad (3)$$

Where σ presents the degeneracy of the reaction pathway, Γ(T) is the tunneling correction factor approximated by Wigner approach [38], k_B is the Boltzmann's constant, T is the temperature, h represents the Planck's constant, and $\triangle_+^{\ddagger} G$ is the Gibbs free energy of activation and v_i is the imaginary frequency, whose vibrational motion is the direction of the reaction.

3. Results and discussion

3.1 Determining optimal values of electrochemical parameters on NAX removal

The catalyst concentration is an important parameter in the EF processes that strongly influences organic pollutants removal efficiency [22]. The optimized concentration of ferrous iron was varied from 0.05 to 0.5 mM (Fig. 1) in the EF process with Pt anode (EF-Pt). The maximum degradation rate of NAX was obtained for a catalyst concentration of 0.10 mM. Interestingly, the NAX oxidation rate catalyst led to increase in the rate of the competitive reaction between Fe^{2+} and $^{\bullet}OH$ (Eq. (4)) causing a lower NAX degradation efficiency [39, 40].

$$Fe^{2+} + {}^{\bullet}OH \rightarrow Fe^{3+} + OH^{-} \quad (4)$$

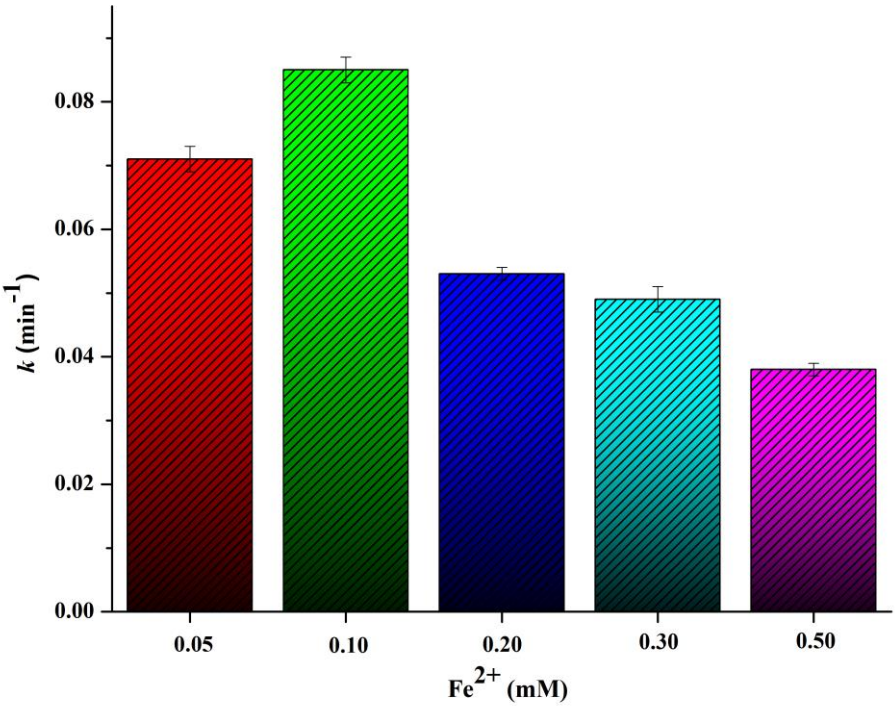

Fig. 1. ***Apparent rate constant of naproxen oxidation by $^{\bullet}OH$ at different concentration of ferrous ion (catalyst) in tap water medium by EF-Pt process. $[NAX]_0$ = 0.198 mM; $[Na_2SO_4]$ = 50 mM; V = 0.25 L; pH = 3.0; current intensity: 0.10 A.***

NAX mineralization was found to be dependent to the applied current value as its TOC removal rate. For instance, TOC abatement rate after 4 h of electrolysis was 84.60%, 94.60% and 68.80% at 0.10 A for EF-Pt, EF-BDD and AO-BDD, respectively (Fig. 2). The current is a main parameter for EAOPs since it governs the electrochemical reaction generating •OH in the bulk and on the anode surface. Thus, an applied current intensity ranging from 0.10 to 0.75 A was tested in the EAOPs processes with Pt BDD anodes vs. carbon felt cathode to monitor the degradation and/or mineralization of 0.198 mM NAX. The degradation rates of NAX increased with increasing current values (Fig. 3a). NAX degradation fits well the both pseudo-first order reaction kinetics - k_{app} (R^2>0.981, Table S3) and retarded first-order model (Eq. (5)) kinetics - k_a (R^2>0.940, Table S3) [41].

core-shell particles

$$-\frac{dC_t}{d_t} = \frac{k_a}{1+at}\ C_t \ or\ C_t = C_0\ (1+at)^{-k_a/a} \qquad (5)$$

where C_0 and C_t are NAX concentration (mg L^{-1}) at time 0 and t (min), respectively, k_α is the apparent rate constant (min^{-1}), which is analogous to the initial pseudo-first-order rate constant, and retardation factor α describes the decline of the reaction rate with time.

Higher k_{app} and k_a values were found for EF when compared with AO; specifically, the k_{app} of EF-BDD was about 7-fold higher than that of AO-BDD at same current intensity. The k_{app} values of EF-Pt were lower than that of EF-BDD (Table S2), which is related to the production of supplementary, highly reactive •OH on the surface the BDD (BDD•OH), compared with the Pt anode [42]. Pt anodes have a lower O_2 evolution overpotential, with relatively less Pt(•OH) which are chemisorbed, thus are less reactive. Meanwhile, the higher current values accelerate H_2O_2 and Fe^{2+} formation kinetics and consequently promote •OH generating rate, resulting in higher degradation efficiency of NAX [43].

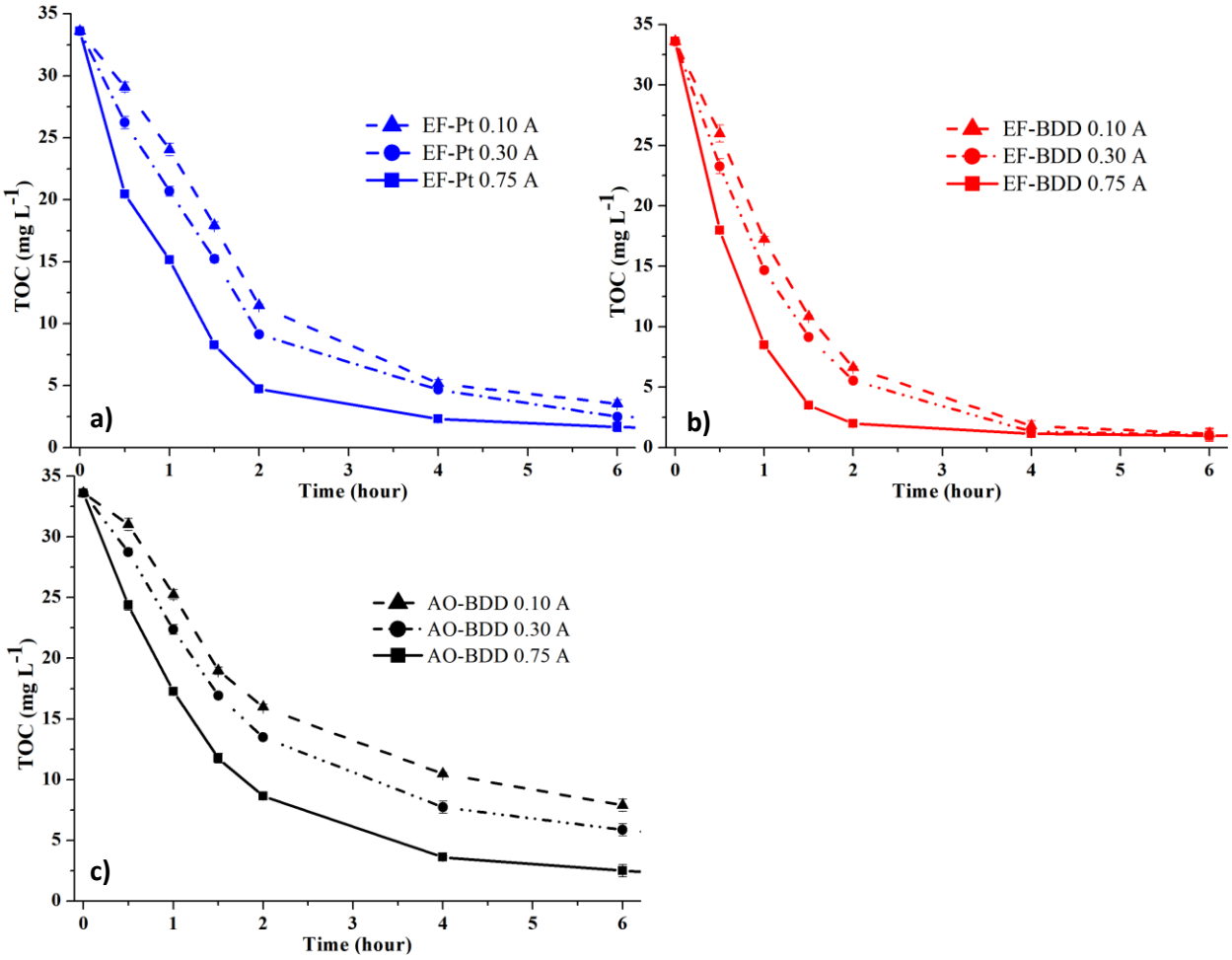

Fig. *2. Effect of applied current intensity on mineralization of naproxen by •OH in tap water during its oxidative degradation by EAOPs.*

Then, TOC removal rate become very low indicating a significantly lower current efficiency. The mineralization current efficiency (MCE) follows the order: EF-BDD > EF-Pt > AO-BDD as shown in Fig. 3b. The lower MCE value decelerated at higher current values can be attributed to: (i) decrease of organic matter in the solution, (ii) the competition between the formation of H_2O_2 with the side reaction of the hydrogen gas evolution (Eq. (6)), (iii) promotion of parasitic reactions consuming •OH (Eqs. (7) and (8)) [44] and (iv) the formation of hard-to-oxidize intermediates, such as carboxylic acids, due to their lower reaction rates with •OH [45]. Therefore, a lower current intensity should be used,

for NAX removal in aqueous systems to avoid adverse effect such low current efficiency and high-energy consumption (Figs. 3b and 3c).

$2\ H_2O + 2\ e^- \rightarrow H_2\ (g) + 2\ OH^-$ (6)

$2BDD(^{\bullet}OH) \rightarrow 2BDD + O_2 + 2H^+ + 2e^-$ (7)

$H_2O_2 + {}^{\bullet}OH \rightarrow HO_2^{\bullet} + H_2O$ (8)

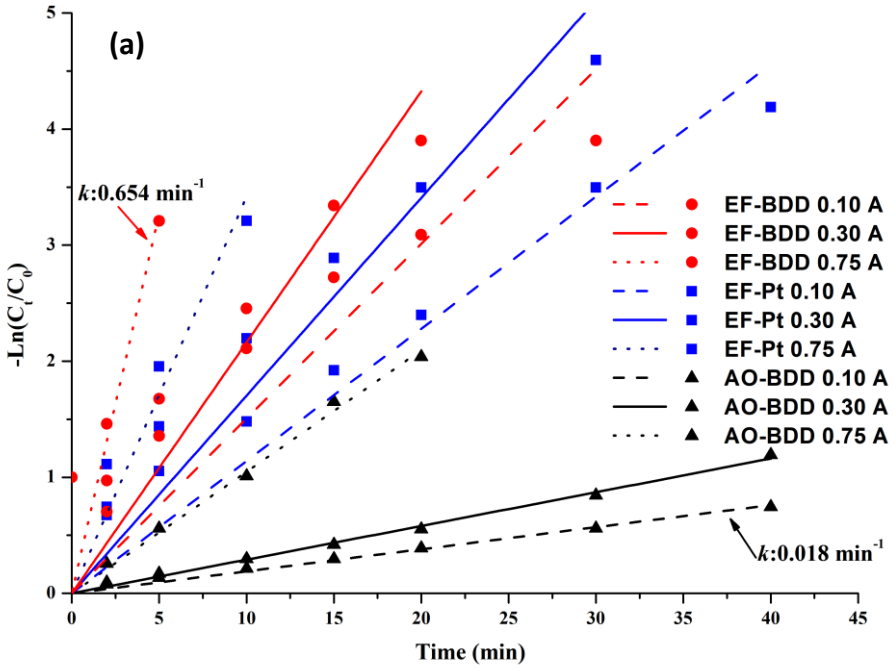

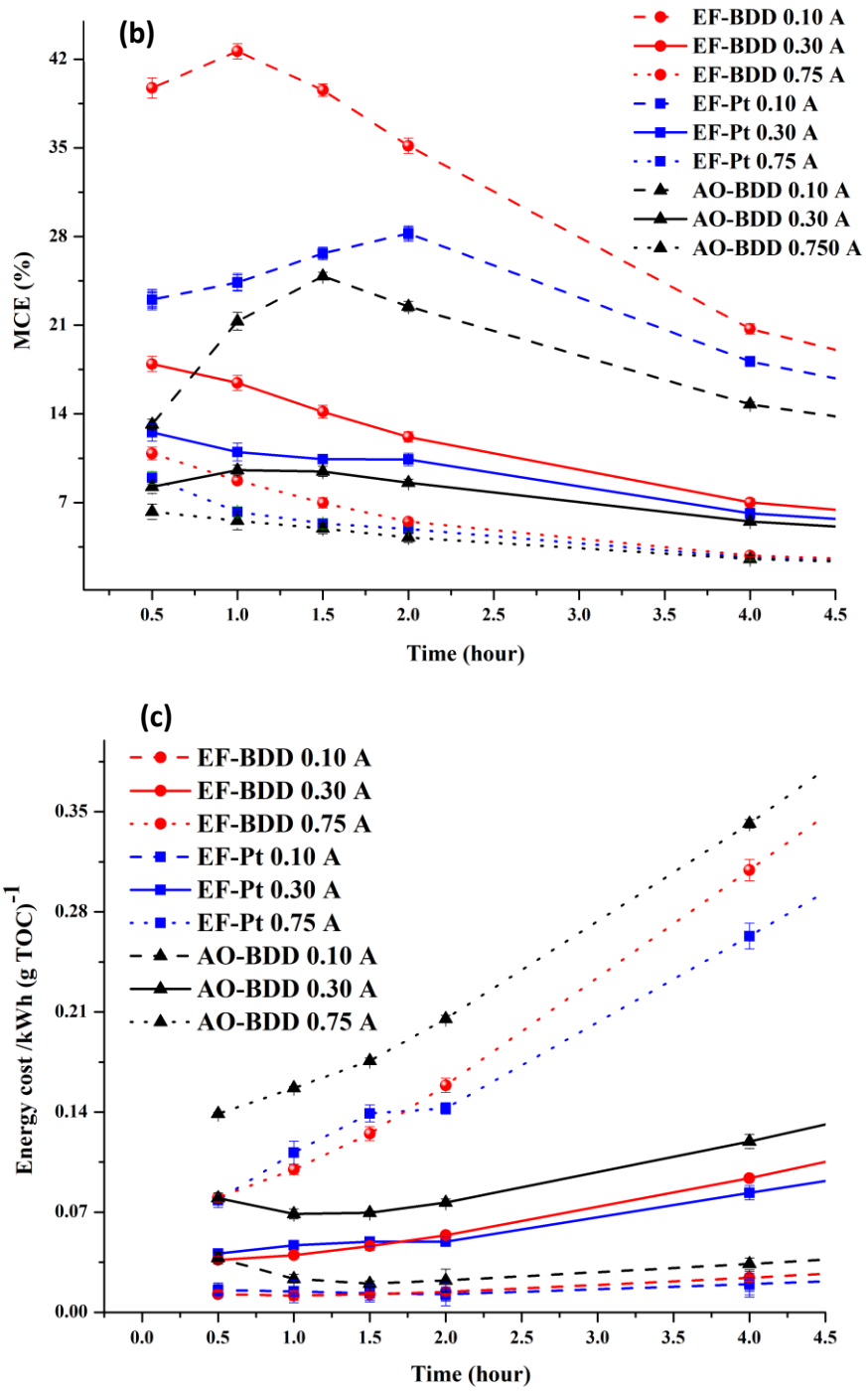

Fig. 3. ***(a): Linear relationship of – Ln(C_t/C_0) and operation time; (b): MCE value (%)of mineralization of NAX by $^{\bullet}OH$ and (c): Energy cost of mineralization of NAX under different current intensities in EAOPs. $[NAX]_0$ = 0.198 mM; $[Na_2SO_4]$ = 50 mM; V = 0.25 L; for EF: $[Fe^{2+}]$ = 0.10 mM; pH = 3.0; for AO: pH = 7.5.***

For the consideration of economic aspect of the treatment, the energy cost (EC) for the tests was

calculated using Eq. (9) [22]:

Energy cost [kWh (g TOC) $^{-1}$] = $\frac{VIt}{\Delta(\mathrm{TOC})\exp \mathrm{Vs}}$ (9)

in which, V is the cell voltage (V), t is the electrolysis time (h), and all other parameters are the same as for Eq. (1). The EC values ranged from 0.012 and 0.036, 0.012 and 0.047, 0.02 and 0.057 kWh (g TOC)$^{-1}$, at 0.10 A, for EF-Pt, EF-BDD and AO-BDD, respectively.

As expected, the EC increases with increasing current intensity (Fig. 3c). Application of AO results in higher costs compared to the EF process, which indicates that trace catalyst iron addition could remarkably reduce the energy input. The lower EC was obtained around 1 to 2 h at 0.10 and 0.30 A, however, with an obvious increase at 0.75 A in all EAOPs. Hence, considering the degradation, mineralization and energy costs we show that the removal of NAX solution could be processed under lower current intensity within the first 2 h.

3.2 Toxicity analysis

The intermediates produced from oxidation of NAX have been often reported to manifest a higher toxicity than the parent molecule itself [46]. Hence, in order to understand the evolution of the toxicity of NAX solution during treatment, bioluminescence measurements were conducted after 15 min exposure to marine bacteria *V. fischeri* with solutions electrolyzed at different constant current intensities (I= 0.10 and 0.30 A) with BDD and Pt anodes at different electrolysis time (Fig. 4). The toxicity evolution of a blank sample (C_0 = 0 mgL^{-1}) was also assessed as reference and used for correction of the presented results.

As it can be seen from the curves of this figure, there was a significant increase of luminescence inhibition peaks within 20 min of electrolysis, which clearly showed that highly toxic intermediates

were produced during this interval of treatment. The research showed higher toxic intermediates than the parent molecule (NAX) produced in a different treatment process (i.e., photo-transformation) [47]. Similar results were also obtained by Jallouli et al. [46]. Compared to the initial toxicity level, all the samples displayed a lower percentage of bacteria luminescence inhibition after about 20 min of treatment, indicating that toxic intermediates were eliminated during the treatment.

The luminescence inhibition was higher with lower current intensity values, which is attributed to the lower formation rates of •OH in these processes. At the same current intensity, a higher inhibition was obtained by the application of Pt anode, due to the lower oxidation power of Pt and the slower degradation of the organic matter in solutions, as indicated by the lower TOC abatement. Afterwards, the curves continuously decreased and there was a convergence between the curves of different anodes application, most possibly due to the similar products in the medium for the different processes, i.e., the short-chain carboxylic acids (*vide infra*, section 3.3). These compounds are relatively recalcitrant to •OH but are all biodegradable. A high efficiency on removal of NAX and a decreased toxicity of the treated NAX solution makes EF-BDD process an applicable treatment at high pollutants' concentration from industrial wastewaters.

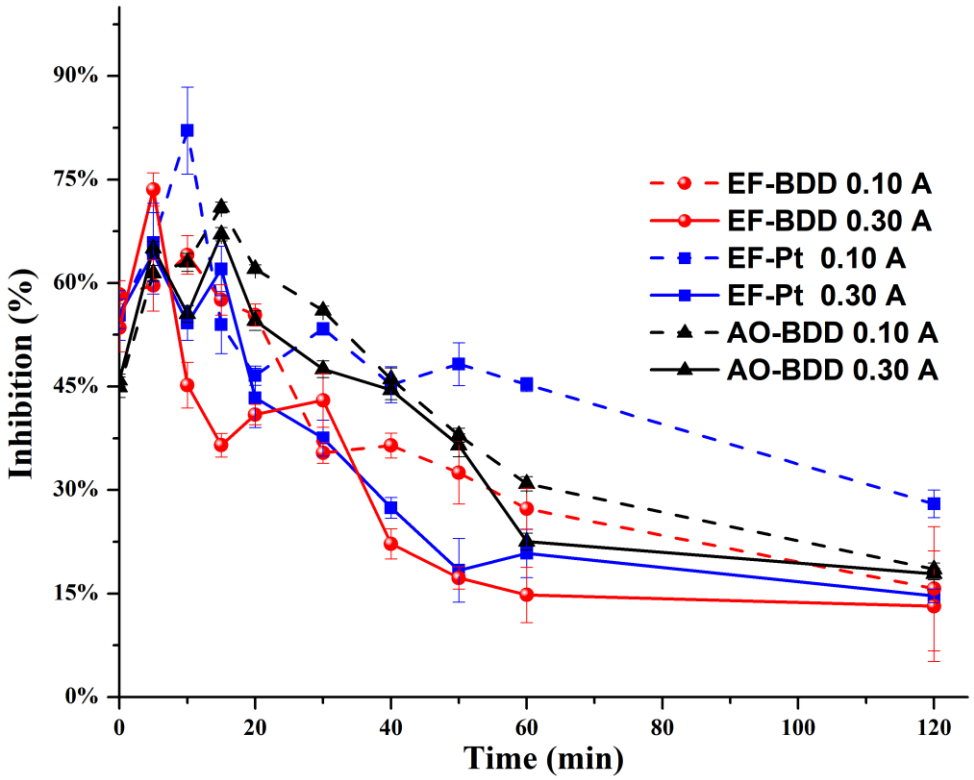

Fig. ***4. Evolution of the inhibition of Vibrio fischeri luminescence (Microtox® test) during EAOPs. [NAX]*** $_0$ ***= 0.198 mM; [Na₂SO₄] = 50 mM; V = 0.25 L; for EF: [Fe²⁺] = 0.10 mM; pH = 3.0; for AO: pH = 7.5.***

3.3 Evolution of the detected mineralization intermediates of naproxen

To investigate the mineralization mechanism of NAX by •OH during EAOPs treatments, the experiments were conducted in deionized water and the resulting intermediates (i.e., aromatic by-products and short-chain carboxylic acids) were identified and quantified by comparison of retention time (t_R) of standards compounds. The intermediates were identified as benzoic acid, hydroquinone, catechol, 3-hydroxybenzoic acid, pyrogallol, phthalic anhydride, phthalic acid, phenol, 1,5-dihydroxynaphthalene, 1-naphthaleacetic, and 2-naphthol, at t_R (min) of 2.97, 3.53, 4.7, 5.0, 5.3, 6.3, 6.9, 7.5, 8.0, 8.7, and 9.8, respectively (Fig. S3a).

Fig. 5a shows that high molecular-weight aromatic intermediates were formed at the early stage of

the electrolysis simultaneously with the disappearance of the parent molecule. 1,5-dihydroxynaphthalene, 2-naphthol, and phenol were first produced; it is well-known that these three compounds have high acute toxicity to aquatic life [48, 49], which explains the higher toxicity occurred in the former processes depicted in Fig. 4. Then, non-toxic compounds as 1-naphthalenacetic and 3-hydroxybenzoic acids appeared. The concentration of most of the aforementioned intermediates was less than 0.017 mM Following, intermediates such as catechol, benzoic acid, phthalic acid, pyrogallol, phthalic anhydride and hydroquinone reached their highest concentration, then decreased gradually within the electrolysis time. These by-products were all formed in small quantities. However, compounds such as catechol, with a higher concentration at late stages of NAX elimination, pinpointed the second peak of luminescence inhibition. All the detected intermediates, except benzoic acid, were completely removed before the total elimination of NAX. Considering that persistent intermediates containing polar functional moieties were formed in Fenton-based reactions, such as hydroxyl and carboxyl groups, they are expected to be highly mobile in environmental systems, despite their high molecular weight.

The concentrations of the produced carboxylic acids were higher than that of aromatics (Fig. 5b), indicating that short-chain carboxylic acids were quickly generated from the oxidative breaking of the aryl moiety of aromatics in the EF process [50, 51]. The elution time for each acid was shown in Fig. S3b. Oxalic and formic acids persisted for longer, being the terminal carboxylic acids that are directly converted into CO_2 [42]. Glycolic and malic acid were identified at the beginning of electrolysis time and disappeared gradually, among which glycolic acid contributed the latter peak of inhibition % of bacteria shown in Fig. 4. Formic acid got to its maximum peak concentration of 0.08 mM after 1 h of electrolysis and then decreased gradually. Glyoxylic acid constantly appeared in the electrolysis time,

below 0.004 mM. Acetic acid was formed as the largest amount acid with its highest amount of 0.076 mM formed after 2 h electrolysis time. Oxalic acid gradually increased to its maximum peak concentration 0.197 mM after 2 h, meaning it can be produced from other carboxylic acids oxidized by •OH (Fig. 5b). The glyoxylic acid may also derive from the oxidation of aryl moieties and then converted to oxalic acid [44]. Oxalic and acetic acids were persistent as the final intermediates during the whole processes. The lack of complete mineralization of NAX by the EF processes can be explained by the ferric-oxalate complexes, which are formed by terminal intermediates reaction with the ferric iron and are resistant to oxidation [52, 53].

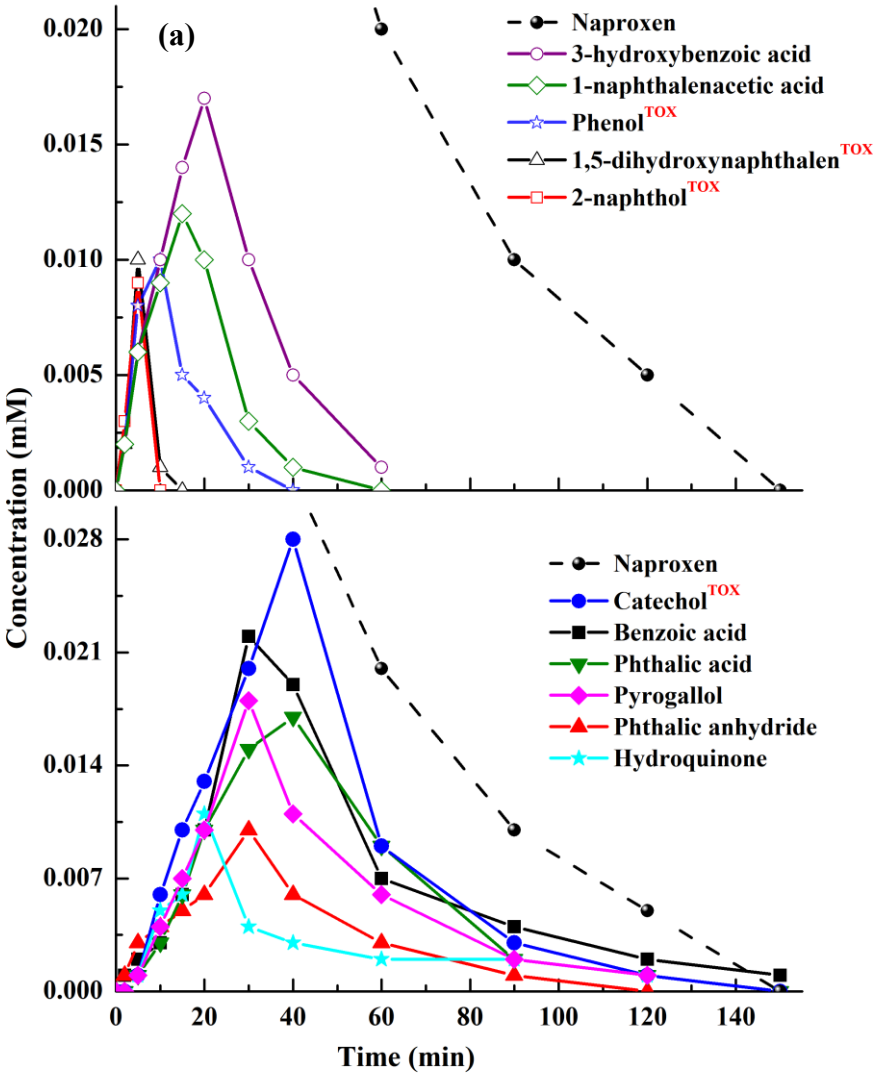

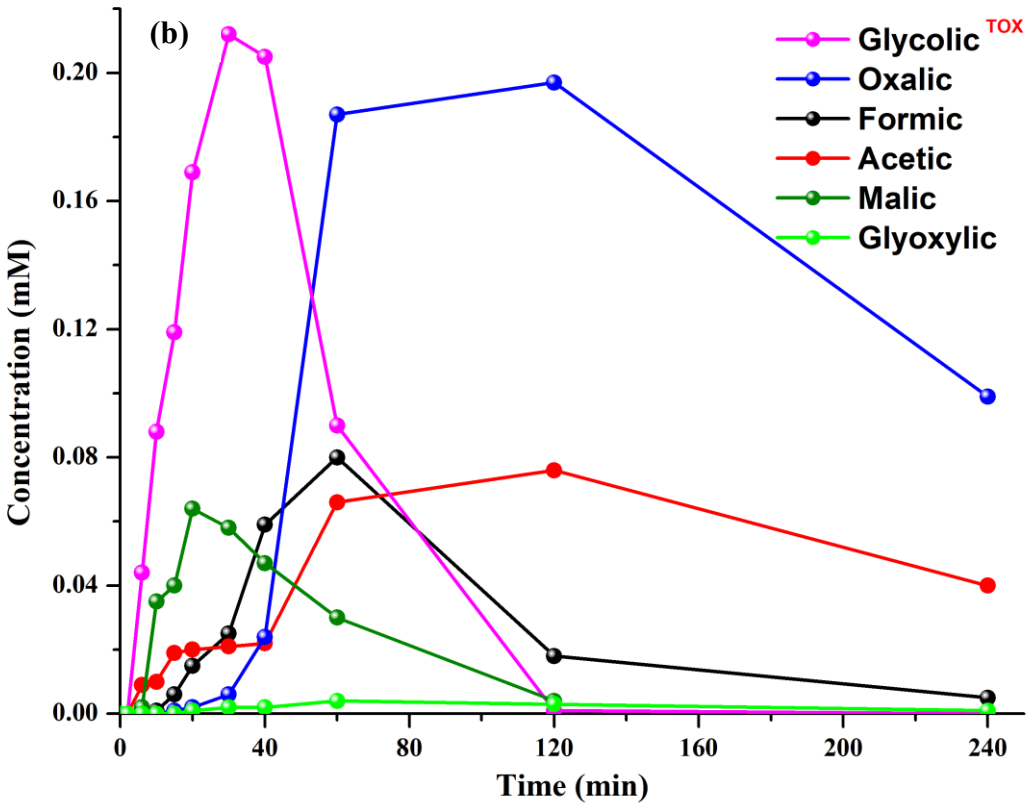

Fig. 5. ***Time course of the concentration of the main aromatic intermediates (a), and short chain carboxylic acids (b) accumulated during degradation of NAX in tap water medium: electro-Fenton process with Pt as anode. [NAX]*** $_0$ ***= 0.198 mM; [*** Na_2SO_4 ***] = 50 mM; V = 0.25 L; [*** Fe^{2+} ***] = 1 mM; pH = 3.0; current intensity = 50 mA.***

3.4 DFT calculation of undetected intermediates oxidized by •OH

DFT calculations were used to systematically compute the intermediates of NAX produced by •OH in the separate pathways of "ring-opening" and "side-chain". The optimized structure of NAX is represented in Fig. S4.

The intermediate and transition states of the first step reaction between NAX and •OH at branched chain have been well investigated in the study of Luo [30]. The "side-chain" reaction by •OH were investigated in our research at first part at possible site of NAX or intermediates of NAX.

3.4.1 Reaction at C_7, C_{12}, and C_{17} of NAX

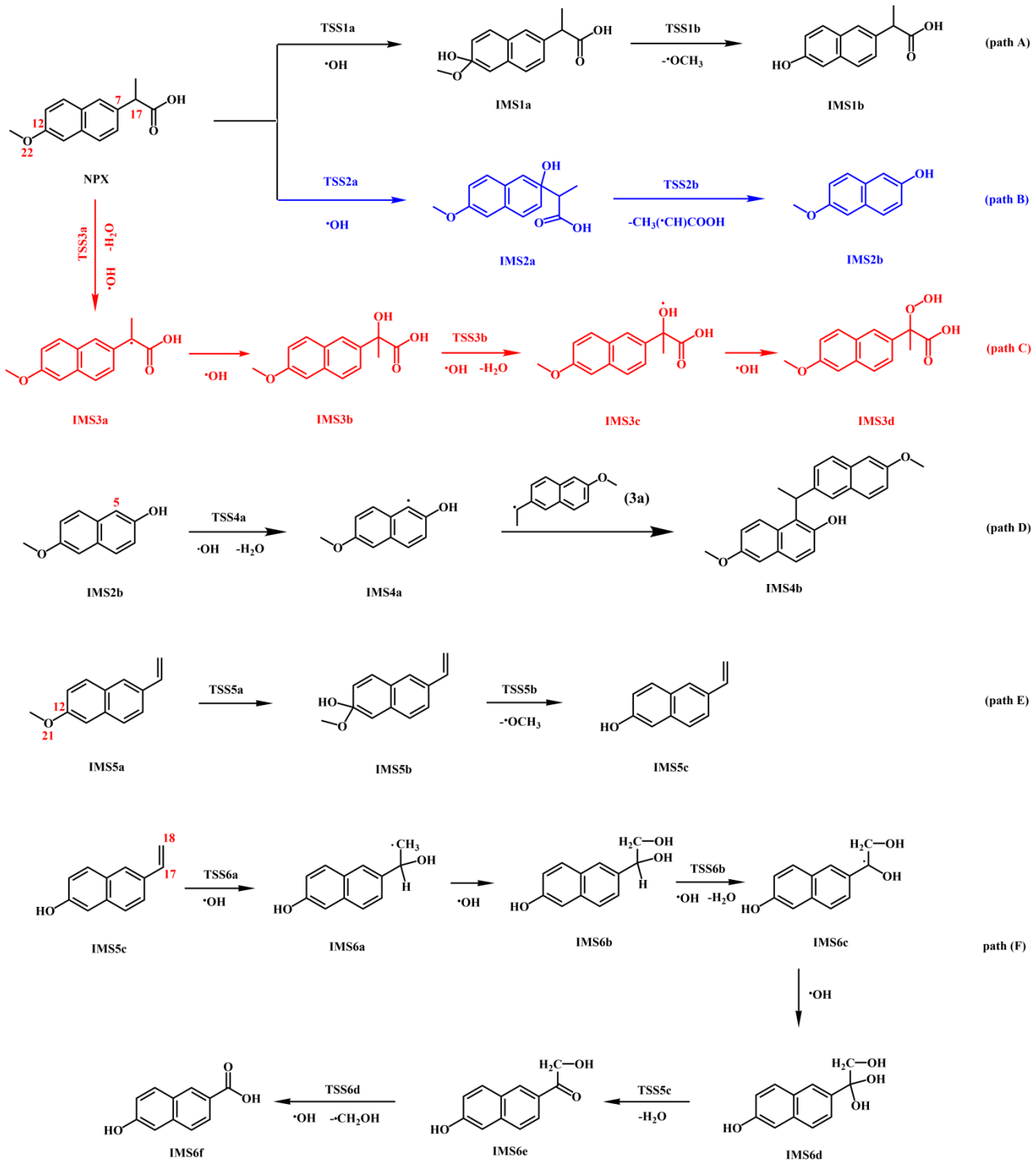

Fig. *6. "Side-chain" reaction of •OH and NAX with calculated intermediates at C_7, C_{12}, and C_{17} (path A-C); C_5*

(path D); C_{12} and C_{22} (path E); and C_{17} and C_{18}.(path F).

•OH attacked C_{12} (black) and C_7 (blue) of naphthalene, leading the formation of IMS1a and IMS2a, forming the new C_{12}-O and C_7-O at branched chain in NAX separately (Fig. 6 path A & B), the corresponding Gibbs free energy change ΔG of IMS1a and IMS2a are ΔG_{S1a} = 5.78 Kcal mol^{-1} and ΔG_{S2a} = 9.46 Kcal mol^{-1} (Fig. S5a & b), respectively, which are consistent with Luo [30]. The corresponding second-order rate constants $k_{S1a} = 3.58 \times 10^{10}$ $s^{-1}m^{-1}$, and $k_{S2a} = 7.21 \times 10^7$ $s^{-1}m^{-1}$.

IMS1a was further oxidized at C_{12}-O_{22} with -O-CH_3 broken off, of ΔG_{S1b} = 11.21 Kcal mol^{-1}, and k_{S1b} = 3.80×10^4 s^{-1}, forming IMS1b- 6-Desmethylnaproxen [11]; IMS2a oxidized at C_7-C_{17} with -CH-CH_3-COOH off, of ΔG_{S2b} = 12.16 Kcal mol^{-1}, and $k_{S2b} = 7.58 \times 10^3$ s^{-1}, forming IMS2b - 6-Methoxy-2-naphthol (Fig. S5a & b) [54].

•OH attacked C_{17} of the branched chain of NAX, producing IMS3a radical (Fig. 6 path C & Fig. S5c), of ΔG_{S3a} = 21.04 Kcal mol^{-1}, and $k_{S3a} = 2.12 \times 10^{-1}$ $s^{-1}m^{-1}$. Furthermore, one •OH added in the C_{17} with the formation of IMS3b, which is dehydrated to produce active IMS3c, of ΔG_{S3b} = 1.54 Kcal mol^{-1}, and k_{S3b} = 4.58×10^{13} $s^{-1}m^{-1}$. The generated IMS3c radical combines with •OH at the active O to form IMS3d. It has been well illustrated that IMS3d - 2-hydroperoxy-2-(6-methoxynaphthalen-2-yl) propanoic acid, produced the Ketone derivatives by further dehydration and decarboxylation, as an important intermediate in the oxidative degradation of NAX.

The results show that the de-methoxylation reaction rate (k_{S1a}) of NAX oxidized by •OH is significantly faster than that of de-propionylation reaction rate (k_{S2a}). That is due to the difference of electronegativity of the O atom of -O-CH_3 and that of the C atom of -CH-CH_3-COOH, implying that -O-CH_3 connecting the naphthalene ring has higher electron-donating ability. Therefore, the path A is considered as a primary channel.

3.4.2 Reaction at C_5 of intermediates of NAX

Following, IMS2b produced in the reaction of "path B" was oxidized to active IMS4a, and H_2O, under the activation of •OH with the extraction of H at C_5 (Fig. 6 path D), of ΔG_{S4a} = 3.53 Kcal mol^{-1}, and k_{S4a} = 1.60 × 10^{12} $s^{-1}m^{-1}$ (Fig. S5d). Immediately, IMS4a reacts with molecular named as 3a identified in the oxidation process of NAX in other literature [28], and transfers into a macro-molecular IMS4b (6-Methoxy-1-[1-(6-methoxynaphthalen-2-yl) ethyl] naphthalen-2-ol). IMS4b was detected in the study of Yang [55] and Jallouli [46], proved to be more toxic than the parent NAX, leading to increased toxicity in the early stage of the oxidation process.

3.4.3 Reaction at C_{12} and O_{22} of intermediates of NAX

IMS5a formed by •OH oxidation of NAX was confirmed by Tu [28]. In this paper, the following oxidants produced of IM5Sa by •OH reaction were calculated (Fig. 6 path E & Fig. S5e). IMS5b was formed of one -OH added at C_{12} of IM5Sa, of ΔG_{S5a} = 6.45 Kcal mol^{-1}, and k_{S5a} = 1.16 × 10^{10} $s^{-1}m^{-1}$. Owing to the change of electron-donating ability, •OH attacked the same position, C_{12}-O_{22} bond was broken and demethoxylation reaction happened. IMS5c - 6-Vinylnaphthalen-2-ol [56] was produced in the hydroxylation process of NAX, of ΔG_{S5b} = 14.54 Kcal mol^{-1}, and k_{S5b} = 1.37 × 10^2 s^{-1}.

3.4.4 Reaction at C_{17} and C_{18} of intermediates of NAX

IMS5c obtained above was further oxidized by •OH (Fig. 6 path F & Fig. S5f). •OH firstly attacked the double bond of C_{18} to form pre-intermediate IMS6a_0, leading to the reduction of energy, then transfers into C_{17} to have active IMS6a generated, of ΔG_{S6a} = 29.45 Kcal mol^{-1}, and k_{S6a} = 1.63 × 10^{-7} $s^{-1}m^{-1}$. •OH continues to attack active C_{18} to form IMS6b and then reacts with H connected of C_{17}, leading to dehydration reaction, i.e. one molecular H_2O was off from IMS6b, of ΔG_{S6b} = 7.59 Kcal mol^{-1}, and k_{S6b} = 1.70 × 10^9 $s^{-1}m^{-1}$, forming the active IMS6c. The active IMS6c reacts with •OH, forming one -OH added at C_{17}-IMS6d, that significantly reduces the energy barrier, of ΔG_{S6d} = 37.41 Kcal mol^{-1}

[1], and k_{S6d} = 2.41 × 10^{-15} s^{-1}. The -OH group connected to C_{17} undergoes intermolecular dehydration to form IMS6e. Under the oxidation of •OH, IMS6f -6-Hydroxy-2-naphthoic acid, was formed by one •CH_2OH off from IMS6e, of ΔG_{S6e} = 0.22 Kcal mol^{-1}, and k_{S6e} = 4.22 × 10^{12} s^{-1}. IMS6f obtained is an important oxidation product in the degradation of NAX as previous works indicated [12, 57].

3.4.5 Reaction at C_9-C_{12}, C_{12}-C_{14} and C_2-C_7, C_5-C_7 of "ring-opening" of NAX

•OH has strong oxidization ability as its element O reacted with the C of naphthalene ring, opening the "ring" of NAX. The ortho- methoxy- group in NAX makes the "opening" process easier [58]. In the calculation of branched chain reaction, it is proved that ΔG of attacking C_{12} was lower than that of C_7 by •OH. The sites near methoxy group were calculated as the reacted sites at 3.4.1. Hence, ortho-position of C_{12} as C_9 and C_{14}, and of C_7 as C_2 and C_5, that connect to methoxy group of IMS1a, were calculated.

•OH attacked C_{12}, making the whole naphthalene ring becoming a large active free radical group, forming C-O bond IMS1a. The calculated results demonstrated that the formation of IMS1a is no energy barrier. •OH attacked sites of adjacent C_9 and C_{14} to C_{12} and then generated the corresponding stable intermediates IMR1a and IMR2a (Fig. 7 path G & H). These intermediates continued being oxidized by •OH, form coupled structures IMR1a_0 and IMR2a_0, respectively. IMR1a0 reacted with •OH at C_9, with one hydroxylic hydrogen extracted, IMR1b generated, of ΔG_{R1a} = 16.23 Kcal mol^{-1}, and k_{R1a} = 7.97 × 10^2 $s^{-1}m^{-1}$; the same reaction occurred at C_{14} of IMR2a_0, to formed IMR2b, of ΔG_{R2a} = 33.11 Kcal mol^{-1}, and k_{R2a} = 3.40 × 10^{-10} $s^{-1}m^{-1}$ (Fig. S5 g & h).

Following, the bound-breaking reaction of C_9-C_{12} and C_{12}-C_{14} bonds implied that "ring-opening" of NAX occurred, with the generation of IMR1c and IMR2c, of ΔG_{R1b} = 0.66 Kcal mol^{-1}, and ΔG_{R2b} = 6.33 Kcal mol^{-1}, respectively. The corresponding reaction rates are k_{R1b} = 2.05 × 10^{12} s^{-1} and k_{R1b} = 1.43 ×

10^8 s^{-1}, IMS2a was formed after •OH attacked the C_7 (Fig. 7 path I). The calculated ΔG of C_2 reaction with •OH was so high that further research ended. On the contrary, a coupling IMR3a0 was formed from the reaction of IMS2a and •OH firstly, and then, •OH attacked C_5 to form IMR3a, of ΔG_{R3a} = 6.80 Kcal mol^{-1}, and k_{R3a} = 4.13 × 10^9 $s^{-1}m^{-1}$. Hydroxyl hydrogen connected with C_5 was extracted through the reaction of •OH and TSR3b, to produce the IMR3b and H_2O, of ΔG_{R3b} = 0.78 Kcal mol^{-1}, and k_{R3b} = 1.64 × 10^{14} $s^{-1}m^{-1}$. TSR3c was formed under the continuous oxidation of IMR3b. Then the bond of C_5-C_7 was broken in the oxidative reaction of TSR3c, forming the IMR3c, of ΔG_{R3c} = 2.63 Kcal mol^{-1}, and k_{R3c} = 7.35 × 10^{10} $s^{-1}m^{-1}$. (Fig. S5i)

By using Becke method of the multiwfn program, the spin population is obtained:

(1) IM1R1c, the spin population of C_{12} and C_{16} are 0.26 and 0.38 respectively, which are the higher of all atoms. Based on this data, the optimal resonance formula of IM1R1c is obtained;

(2) IMR2c, the spin population of C_{16} and O_{34} are as high as 0.46 and 0.21, respectively. Based on the spin population, the optimal resonance formula of IMR2c structure is achieved;

(3) Similarly, for IMR3c, the spin population of C_4 and C_7 are 0.39 and 0.31, respectively, the optimal resonance formula of IMR3c is got.

It is clear that the “ring-opening” molecules as IMR1c, IMR2c and IMR3c occurred at the •OH oxidation process of NAX were all of such lower ΔG and short time (nanoseconds level). The three “ring opening” pathways of NAX provide a feasible degradation mechanism.

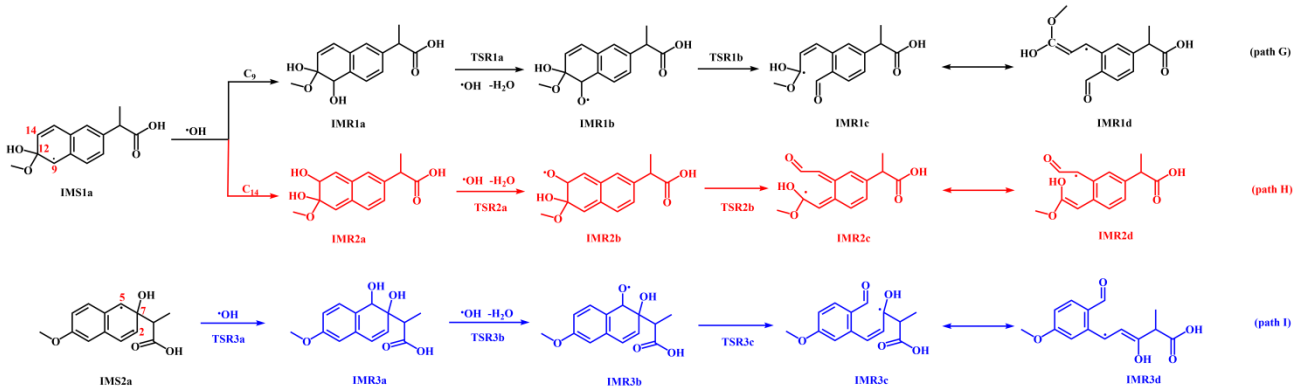

Fig. *7. "Ring-opening" reaction of •OH and NAX at C_{17} and C_{18} with calculated intermediates (path G-I).*

With the electron-donating methoxy group, the C_{12} reacted with •OH of an obviously lower ΔG in path A, leading a primary reacted intermediate. All data of ΔG show that each path of NAX can occur under the attack of •OH. It is worth noting that ΔG of TSS6d in path F and TSR2a in path H are 37.41 Kcal mol^{-1} and 33.11kcal Kcal mol^{-1}, respectively. However, free radicals are coupled in the former step of the reaction, releasing a large amount of energy to overcome the reaction requirements. At the same time, the change of ΔG indicates the rationality of the reaction and the feasibility of theoretical calculation.

3.5 The mechanism of Naproxen removal by •OH

Based on the intermediates (aromatic and carboxylic acids) detected by experimental analysis, the main intermediates substantiated by computation in our work, as well as the intermediates formed upon oxidation of NAX on related literature published [59], the detailed degradation pathway of NAX oxidized by •OH was illustrated in Fig. 8.

The reactions of •OH on NAX happen as decarboxylation, hydroxylation, demethylation, yielding the molecular as other literature illustrated and DFT calculated (mostly black and blue ones). It was clear that the naphthalic acid and "ring-opening" molecule were formed at the early stage of the

electrolysis. Aromatic intermediates are generated concomitantly with the disappearance of the parent molecule. Side chain on the C(β)-atom of polycyclic aromatic hydrocarbons was oxidized to form intermediates. In parallel, hydroxylation led to hydroxyl-rich polycyclic aromatic hydrocarbons. The attack of •OH on NAX happened by addition of •OH on the benzoic ring (hydroxylation) or by losing side chain. These intermediates were then oxidized to form polyhydroxylated products that finally underwent oxidative ring opening reactions, leading to the formation of aliphatic compounds. Further reaction with the cleavage of the aromatic ring in the electron-rich benzene formed hydroxylated benzenes as di/tri-hydroxybenzenes of corresponding as 3-hydroxybenzoic acid, phenol, catechol, benzoic acid, phthalic, pyrogallol, phthalic anhydride and hydroquinone etc. (mostly top green ones). Finally, these intermediates were mineralized to carbon dioxide by further reactions with •OH, as acetic, oxalic, formic, glycolic, malic and succinic acids, which originate from the oxidative breaking of the benzenes' moiety of aromatic intermediates. In the end, the final carboxylic acids were oxidized to carbon dioxide and water, or oxalic acid which formed hardly oxidizable iron complexes.

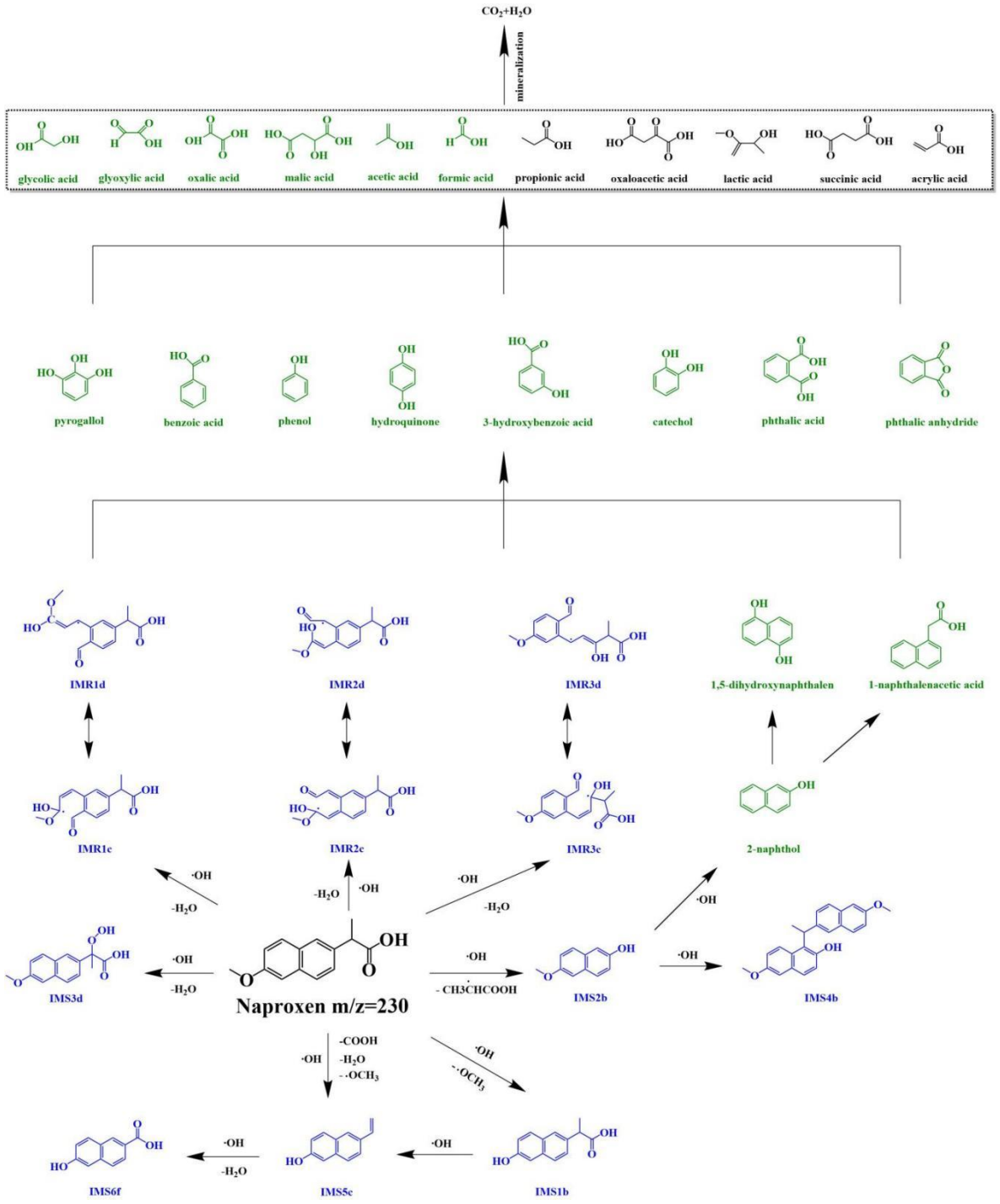

Fig. 8. ***General reaction pathway proposed for the mineralization of naproxen in aqueous medium by •OH. Blue: DFT calculated; Green: detected in this research; Black: carboxylic acids validated by other research works.***

3.6 Application of EAOPs on removal of Naproxen in relevant water matrices

To evaluate the applicability of the EAOPs to degrade NAX in matrices more complex than tap water, the pollutant treatment was carried out in simulated urine and wastewater (Table 1). These matrices were considered as the main excretion way of this pharmaceutical in humans is the urine [60, 61], and hospital wastewater is a recognized source of anti-inflammatories discharge into municipal treatment plants [62, 63]. Moreover, the application at primary sources of pollution by NAX (as urine and hospital wastewaters) could contribute to mitigate the negative environmental impact of this pharmaceutical [64].

The k_{app} value of all the experiments were shown in Table S4, in which curves of 0.30 A were selected to present the degradation of NAX in artificial urine and wastewater in Fig. 9. The degradation of NAX in both urine and wastewater was slower than in tap water. This is most likely associated to the presence of competing substances in these matrices. Urine contains urea, acetate, chloride, sulfate, phosphate anions at high concentrations, which can react with electro-generated $^{\bullet}OH$ [65], producing less powerful and more selective oxidizing agents (e.g., $Cl^{\bullet}$, $SO_4^{\bullet-}$, $H_2PO_4^{\bullet-}$) than the hydroxyl radical. Also, wastewater has urea, peptone, chloride, sulfate and phosphate anions in higher concentrations than NAX. This explains why the removal in urine and wastewater required more treatment time than in tap water.

However, the EAOPs were able to reach 100% of degradation even in these complex matrices (which have elevated concentrations of competing substances) after 2 h of treatment, compared with 30~60 min in tap water. As the experimental parameters show, the naturally occurring iron contents in wastewater can efficiently remove NAX; this phenomenon indicates that extra iron sludge is not expected in a potential real application. A moderate hydraulic retention time (2 h), and a low current

intensity applied (0.3 A) were sufficient to eliminate pollutants from complex matrices.

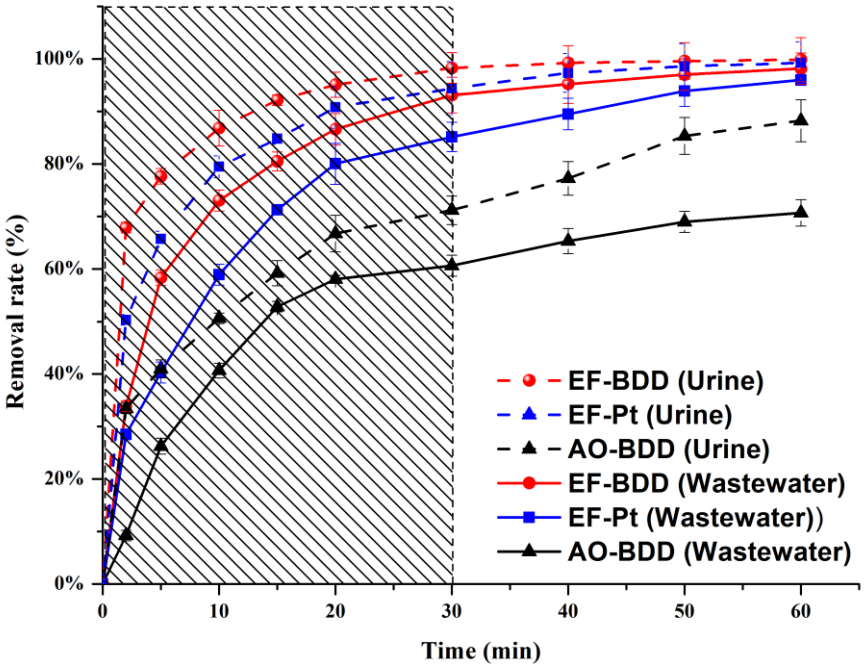

Fig. 9. ***Degradation of NAX by •OH in urine and wastewater. C_0 = 0.198 mM; [Na_2SO_4] = 50 mM; V = 0.25 L; current intensity: 0.30 A; for EF: [Fe^{2+}] = 0.2mM; pH = 3.0; for AO: pH = 7.5.***

4. Conclusions

In this work, the removal of NAX in aqueous solution was carried out with BDD/Pt as anode and carbon-felt as cathode at lab-scale. It has been found out that 0.198 mM NAX could be almost completely eliminated in all EAOPs, with an optimized ferrous ion concentration at natural level in EF processes. In addition, the increasing current intensity accelerates the degradation and mineralization processes. The degradation curves of NAX by hydroxyl radicals within electrolysis time followed pseudo-first order reaction kinetics. EF with BDD anode showed higher removal ability as additional $^{\bullet}OH$ due to the Fenton reaction, a large surface area and higher ability of the BDD anode, compared with AO-BDD and EF-Pt, separately.

The “ring-opening” intermediates of NAX were firstly proposed by theoretical DFT calculation. Based on the intermediates identified during the treatment and DFT calculation, an oxidation pathway of NAX by $^{\bullet}OH$ was proposed. The evolution of intermediates and toxicity is summarized as: the aromatic intermediates were oxidized at the early stage by addition of $^{\bullet}OH$ on the benzoic ring (hydroxylation) or by losing side chain, which cause the increase of the inhibition of the luminescence of bacteria *Vibrio fischeri* by phenol, 1,5-dihydroxynaphthalen, 2-naphthol, catechol and IMS4b. Then, the short chain carboxylic acids were produced from the cleavage of the aryl moiety, such as glycolic, malic, succinic acids. The non-electrolyzed solution explained the remaining TOC observed within the electrolysis time. This explained why a high MCE value was obtained at low current intensity, where the side reaction and energy loss occurred on the persistent small byproducts produced. EAOPs were able to reach 100% of NAX degradation in artificial urine and hospital wastewater in 2 hours of treatment with a low current intensity applied.

Considering the energy input, removal efficiency and toxicity evaluation, less than a 2-h application

is necessary for NAX elimination in different water matrices. Hence, it can be concluded that the EF with BDD anode process could efficiently and quickly eliminate NAX and aromatic intermediates, while AO-BDD can be applied at neutral pH and with no catalyst input. Therefore, except the efficiency, economic input, duration of treatment or other requirements need to be taken into account when making the choice of EAOPs in real applications.

In overall, our results point out that i) EAOPs can be great in NAX removal, ii) even challenging matrices can be properly treated, iii) oxidation of NAX can lead to the generation of more toxic by-products, but prolonged treatment decreases this effect, iv) partial treatment can be risky, according to the expected intermediates formed, v) high-degree mineralization always ensures toxicity loss, and vi) DFT is a powerful tool to predict the intermediates and their toxicity, since complete mineralization is not always feasible and partially treated matrices are often discharged. Further assessment of the elicited toxicity phenomena must be performed; we should underline that despite the utility of *V. fischeri* as a model bacterium indicator of acute toxicity, generalization of the results should be made with caution, and the employment of higher order or more complex organisms should be tested before extrapolating these results towards expressing human toxicity concerns.

Acknowledgements

This work was supported by European Commission for providing financial support through the Erasmus Mundus Joint Doctorate Programme ETeCoS^3 (Environmental Technologies for Contaminated Solids, Soils and Sediments) under the grant agreement FPA n°2010-0009, National Natural Science Foundation of China (No. 42067032), and China Scholarship Council (CSC: 201708155010). Stefanos Giannakis acknowledges the Spanish Ministry of Science, Innovation and Universities (MICIU) for the Ramón y Cajal Fellowship (RYC2018-024033-I).

References

[1] S. Fekadu, E. Alemayehu, R. Dewil, B. Van der Bruggen, Pharmaceuticals in freshwater aquatic environments: A comparison of the African and European challenge, Sci. Total Environ. 654 (2019) 324-337. https://doi.org/10.1016/j.scitotenv.2018.11.072.

[2] M. Parolini, Toxicity of the Non-Steroidal Anti-Inflammatory Drugs (NSAIDs) acetylsalicylic acid, paracetamol, diclofenac, ibuprofen and naproxen towards freshwater invertebrates: A review, Sci. Total Environ. 740 (2020) 140043. https://doi.org/10.1016/j.scitotenv.2020.140043.

[3] P. Grenni, L. Patrolecco, N. Ademollo, A. Tolomei, A. Barra Caracciolo, Degradation of Gemfibrozil and Naproxen in a river water ecosystem, Microchem. J. 107 (2013) 158-164. https://doi.org/10.1016/j.microc.2012.06.008.

[4] P. Sehonova, L. Plhalova, J. Blahova, V. Doubkova, M. Prokes, F. Tichy, E. Fiorino, C. Faggio, Z. Svobodova, Toxicity of naproxen sodium and its mixture with tramadol hydrochloride on fish early life stages, Chemosphere 188 (2017) 414-423. https://doi.org/10.1016/j.chemosphere.2017.08.151.

[5] Y. Wang, B. Jing, F. Wang, S. Wang, X. Liu, Z. Ao, C. Li, Mechanism Insight into enhanced photodegradation of pharmaceuticals and personal care products in natural water matrix over crystalline graphitic carbon nitrides, Water Res. 180 (2020) 115925. https://doi.org/10.1016/j.watres.2020.115925.

[6] M. Manrique-Moreno, M. Suwalsky, F. Villena, P. Garidel, Effects of the nonsteroidal anti-inflammatory drug naproxen on human erythrocytes and on cell membrane molecular models, Biophys. Chem. 147(1-2) (2010) 53-8. https://doi.org/10.1016/j.bpc.2009.12.010.

[7] K. Kwak, K. Ji, Y. Kho, P. Kim, J. Lee, J. Ryu, K. Choi, Chronic toxicity and endocrine disruption of naproxen in freshwater water fleas and fish, and steroidogenic alteration using H295R cell assay, Chemosphere 204 (2018) 156-162. https://doi.org/10.1016/j.chemosphere.2018.04.035.

[8] D. Wojcieszynska, U. Guzik, Naproxen in the environment: its occurrence, toxicity to nontarget organisms and biodegradation, Appl. Microbiol. Biotechnol. 104(5) (2020) 1849-1857. https://doi.org/10.1007/s00253-019-10343-x.

[9] Y. Wu, X. Jin, Y. Liu, S. Huang, F. Wang, X. Zheng, D. Wei, H. Liu, P. Chen, G. Liu, Facile synthesis of solar light-driven Z-scheme Ag_2CO_3/TNS-001 photocatalyst for the effective degradation of naproxen: Mechanisms and degradation pathways, Sep. Purif. Technol. 254 (2021) 117598. https://doi.org/10.1016/j.seppur.2020.117598.

[10] J.C. Lancheros, C.A. Madera-Parra, A. Caselles-Osorio, W.A. Torres-López, X.M. Vargas-Ramírez, Ibuprofen and Naproxen removal from domestic wastewater using a Horizontal Subsurface Flow Constructed Wetland coupled to Ozonation, Ecol. Eng. 135 (2019) 89-97. https://doi.org/10.1016/j.ecoleng.2019.05.007.

[11] K. Kolecka, M. Gajewska, S. Cytawa, P. Stepnowski, M. Caban, Is sequential batch reactor an efficient technology to protect recipient against non-steroidal anti-inflammatory drugs and paracetamol in treated wastewater? Bioresour. Technol. 318 (2020) 124068. https://doi.org/10.1016/j.biortech.2020.124068.

[12] B. Ren, X. Shi, X. Jin, X.C. Wang, P. Jin, Comprehensive evaluation of pharmaceuticals and personal care products (PPCPs) in urban sewers: Degradation, intermediate products and environmental risk, Chem. Eng. J. 404 (2021) 127024. https://doi.org/10.1016/j.cej.2020.127024.

[13] M.A. Oturan, J.-J. Aaron, Advanced Oxidation Processes in Water/Wastewater Treatment: Principles and Applications. A Review, Crit. Rev. Environ. Sci. Technol. 44(23) (2014) 2577-2641. https://doi.org/10.1080/10643389.2013.829765.

[14] Y. Liu, Y. Tang, Y. Wu, L. Feng, L. Zhang, Degradation of naproxen in chlorination and UV/chlorine processes: kinetics and degradation products, Environ. Sci. Pollut. Res. 26(33) (2019) 34301-34310. https://doi.org/10.1007/s11356-019-04472-z.

[15] C.E.S. Paniagua, I. Amildon Ricardo, E.O. Marson, B.R. Gonçalves, A.G. Trovó, Simultaneous degradation of the pharmaceuticals gemfibrozil, hydrochlorothiazide and naproxen and toxicity changes during UV-C and UV-C/H_2O_2 processes in different aqueous matrixes, J. Environ. Chem. Eng. 7(3) (2019) 103164. https://doi.org/10.1016/j.jece.2019.103164.

[16] S. Chen, M. Cai, Y. Liu, L. Zhang, L. Feng, Effects of water matrices on the degradation of naproxen by reactive radicals in the UV/peracetic acid process, Water Res. 150 (2019) 153-161. https://doi.org/10.1016/j.watres.2018.11.044.

[17] D. Kanakaraju, C.A. Motti, B.D. Glass, M. Oelgemöller, TiO_2 photocatalysis of naproxen: Effect of the water matrix, anions and diclofenac on degradation rates, Chemosphere 139 (2015) 579-588. https://doi.org/10.1016/j.chemosphere.2015.07.070.

[18] W. Li, V. Nanaboina, Q. Zhou, G.V. Korshin, Effects of Fenton treatment on the properties of effluent organic matter and their relationships with the degradation of pharmaceuticals and personal care products, Water Res. 46(2) (2012) 403-412. https://doi.org/10.1016/j.watres.2011.11.002.

[19] R.J. Lan, J.T. Li, H.W. Sun, W.B. Su, Degradation of naproxen by combination of Fenton reagent and ultrasound irradiation: optimization using response surface methodology, Water Sci. Technol. 66(12) (2012) 2695-701. https://doi.org/10.2166/wst.2012.508.

[20] D.B. Miklos, C. Remy, M. Jekel, K.G. Linden, J.E. Drewes, U. Hübner, Evaluation of advanced oxidation processes for water and wastewater treatment – A critical review, Water Res. 139 (2018) 118-131. https://doi.org/10.1016/j.watres.2018.03.042.

[21] Y. Deng, R. Zhao, Advanced Oxidation Processes (AOPs) in Wastewater Treatment, Curr. Pollut. Rep. 1(3) (2015) 167-176. https://doi.org/10.1007/s40726-015-0015-z.

[22] E. Brillas, I. Sirés, M.A. Oturan, Electro-Fenton Process and Related Electrochemical Technologies Based on Fenton's Reaction Chemistry, Chem. Rev. 109(12) (2009) 6570-6631. https://doi.org/10.1021/cr900136g.

[23] M.H. Zhou, M.A. Oturan, I. Sirés, "Electro-Fenton Process: New Trends and Scale-Up". The Handbook of Environmental Chemistry, Volume 61. Springer, Singapore, 2018, ISBN: 978-981-10-6405-0.

[24] M. Panizza, G. Cerisola, Direct And Mediated Anodic Oxidation of Organic Pollutants, Chem. Rev. 109(12) (2009) 6541-6569. https://doi.org/10.1021/cr9001319.

[25] X. Du, M.A. Oturan, M. Zhou, N. Belkessa, P. Su, J. Cai, C. Trellu, E. Mousset, Nanostructured electrodes for electrocatalytic advanced oxidation processes: From materials preparation to mechanisms understanding and wastewater treatment applications, Appl. Catal. B 296 (2021) 120332. https://doi.org/10.1016/j.apcatb.2021.120332.

[26] P.V. Nidheesh, M. Zhou, M.A. Oturan, An overview on the removal of synthetic dyes from water by electrochemical advanced oxidation processes, Chemosphere 197 (2018) 210-227. https://doi.org/10.1016/j.chemosphere.2017.12.195.

[27] S. Wacławek, Do We Still Need a Laboratory to Study Advanced Oxidation Processes? A Review of the Modelling of Radical Reactions used for Water Treatment, Ecol. Chem. Eng. S 28(1) (2021) 11-28. https://doi.org/10.2478/eces-2021-0002.

[28] N. Tu, Y. Liu, R. Li, W. Lv, G. Liu, D. Ma, Experimental and theoretical investigation on photodegradation mechanisms of naproxen and its photoproducts, Chemosphere 227 (2019) 142-150. https://doi.org/10.1016/j.chemosphere.2019.04.055.

[29] K.A. Musa, L.A. Eriksson, Theoretical study of the phototoxicity of naproxen and the active form of nabumetone, J. Phys. Chem. A 112(43) (2008) 10921-30. https://doi.org/10.1021/jp805614y.

[30] S. Luo, L. Gao, Z. Wei, R. Spinney, D.D. Dionysiou, W.P. Hu, L. Chai, R. Xiao, Kinetic and mechanistic aspects of hydroxyl radical mediated degradation of naproxen and reaction intermediates, Water Res. 137 (2018) 233-241. https://doi.org/10.1016/j.watres.2018.03.002.

[31] M. Skoumal, R.M. Rodríguez, P.L. Cabot, F. Centellas, J.A. Garrido, C. Arias, E. Brillas, Electro-Fenton, UVA photoelectro-Fenton and solar photoelectro-Fenton degradation of the drug ibuprofen in acid aqueous medium using platinum and boron-doped diamond anodes, Electrochim. Acta 54(7) (2009) 2077-2085. https://doi.org/10.1016/j.electacta.2008.07.014.

[32] M.J. Frisch, G.W. Trucks, H.B. Schlegel, G.E. Scuseria, M.A. Robb, J.R. Cheeseman, G. Scalmani, V. Barone, G.A. Petersson, H. Nakatsuji, X. Li, M. Caricato, A.V. Marenich, J. Bloino, B.G. Janesko, R. Gomperts, B. Mennucci, H.P. Hratchian, J.V. Ortiz, A.F. Izmaylov, J.L. Sonnenberg, Williams, F. Ding, F. Lipparini, F. Egidi, J. Goings, B. Peng, A. Petrone, T. Henderson, D. Ranasinghe, V.G. Zakrzewski, J. Gao, N. Rega, G. Zheng, W. Liang, M. Hada, M. Ehara, K. Toyota, R. Fukuda, J. Hasegawa, M. Ishida, T. Nakajima, Y. Honda, O. Kitao, H. Nakai, T. Vreven, K. Throssell, J.A. Montgomery Jr., J.E. Peralta, F. Ogliaro, M.J. Bearpark, J.J. Heyd, E.N. Brothers, K.N. Kudin, V.N. Staroverov, T.A. Keith, R. Kobayashi, J. Normand, K. Raghavachari, A.P. Rendell, J.C. Burant, S.S. Iyengar, J. Tomasi, M. Cossi, J.M. Millam, M. Klene, C. Adamo, R. Cammi, J.W. Ochterski, R.L. Martin, K. Morokuma, O. Farkas, J.B. Foresman, D.J. Fox, Gaussian 16 Rev. A.01, Wallingford, CT, 2016.

[33] L. Goerigk and S. Grimme, Efficient and Accurate Double-Hybrid-Meta-GGA Density Functionals–Evaluation with the Extended GMTKN30 Database for General Main Group Thermochemistry, Kinetics, and Noncovalent Interactions, J. Chem. Theory Comput 7(2)

(2011), 291-309. https://doi.org/10.1021/ct100466k.

[34] F. Weigend and R. Ahlrichs, Balanced basis sets of split valence, triple zeta valence and quadruple zeta valence quality for H to Rn: Design and assessment of accuracy, Phys. Chem. Chem. Phys. 7(18) (2005), 3297-305. https://doi.10.1039/b508541a.

[35] A.V. Marenich, C.J. Cramer, D.G. Truhlar, Universal solvation model based on solute electron density and on a continuum model of the solvent defined by the bulk dielectric constant and atomic surface tensions, J. Phys. Chem. B 113(18) (2009) 6378-96. https://doi.org/10.1021/jp810292n.

[36] H. Ji, W. Liu, F. Sun, T. Huang, L. Chen, Y. Liu, J. Qi, C. Xie, D. Zhao, Experimental evidences and theoretical calculations on phenanthrene degradation in a solar-light-driven photocatalysis system using silica aerogel supported TiO_2 nanoparticles: Insights into reactive sites and energy evolution, Chem. Eng. J. 419 (2021) 129605. https://doi.org/10.1016/j.cej.2021.129605.

[37] R. Xiao, M. Noerpel, H. Ling Luk, Z. Wei, R. Spinney, Thermodynamic and kinetic study of ibuprofen with hydroxyl radical: A density functional theory approach, Int. J. Quantum Chem. 114(1) (2014) 74-83. https://doi.org/10.1002/qua.24518.

[38] E. Wigner, Zeitschrift für physikalische Chemie. Abteilung B: Chemie der Elementarprozesse, Aufbau der Materie, Leipzig: Akademische Verlagsgesellschaft, 1942, p. 203.

[39] L. Feng, N. Oturan, E.D. van Hullebusch, G. Esposito, M.A. Oturan, Degradation of anti-inflammatory drug ketoprofen by electro-oxidation: comparison of electro-Fenton and anodic oxidation processes, Environ. Sci. Pollut. Res. 21(14) (2014) 8406-16.
https://doi.org/10.1007/s11356-014-2774-2.

[40] H. Nadais, X. Li, N. Alves, C. Couras, H.R. Andersen, I. Angelidaki, Y. Zhang, Bio-electro-Fenton process for the degradation of Non-Steroidal Anti-Inflammatory Drugs in wastewater, Chem. Eng. J. 338 (2018) 401-410. https://doi.org/10.1016/j.cej.2018.01.014.

[41] J. Duan, H. Ji, W. Liu, X. Zhao, B. Han, S. Tian, D. Zhao, Enhanced immobilization of U(VI) using a new type of FeS-modified Fe^0 core-shell particles, Chem. Eng. J. 359 (2019) 1617-1628. https://doi.org/10.1016/j.cej.2018.11.008.

[42] N. Oturan, J. Bo, C. Trellu, M.A. Oturan, Comparative Performance of Ten Electrodes in

Electro-Fenton Process for Removal of Organic Pollutants from Water, ChemElectroChem 8(17) (2021) 3294-3303. https://doi.org/10.1002/celc.202100588.

[43] J.E.L. Santos, M.A. Gomez, D.C. Moura, M. Cerro-Lopez, M.A. Quiroz, C.A. Martinez-Huitle, Removal of herbicide 1-chloro-2,4-dinitrobenzene (DNCB) from aqueous solutions by electrochemical oxidation using boron-doped diamond (BDD) and PbO_2 electrodes, J. Hazard. Mater. 402 (2021) 123850. https://doi.org/10.1016/j.jhazmat.2020.123850.

[44] A. Özcan, Y. Şahin, M.A. Oturan, Removal of propham from water by using electro-Fenton technology: Kinetics and mechanism, Chemosphere 73(5) (2008) 737-744. https://doi.org/10.1016/j.chemosphere.2008.06.027.

[45] I. Sirés, E. Brillas, M.A. Oturan, M.A. Rodrigo, M. Panizza, Electrochemical advanced oxidation processes: today and tomorrow. A review, Environ. Sci. Pollut. Res. 21(14) (2014) 8336-8367. https://doi.org/10.1007/s11356-014-2783-1.

[46] N. Jallouli, K. Elghniji, O. Hentati, A.R. Ribeiro, A.M. Silva, M. Ksibi, UV and solar photo-degradation of naproxen: TiO_2 catalyst effect, reaction kinetics, products identification and toxicity assessment, J. Hazard. Mater. 304 (2016) 329-36.
https://doi.org/10.1016/j.jhazmat.2015.10.045.

[47] W.C. Cory, A.M. Welch, J.N. Ramirez, L.C. Rein, Naproxen and Its Phototransformation Products: Persistence and Ecotoxicity to Toad Tadpoles (Anaxyrus terrestris), Individually and in Mixtures, Environ. Toxicol. Chem. 38(9) (2019) 2008-2019. https://doi.org/10.1002/etc.4514.

[48] C. Bretti, C. De Stefano, G. Manfredi, S. Sammartano, Solubility, activity coefficients and acid–base properties of three naphthol derivatives in $NaCl_{(aq)}$ at different ionic strengths and at T=298.15K, J. Mol. Liq. 158(1) (2011) 50-56. https://doi.org/10.1016/j.molliq.2010.10.008.

[49] W.L. Xu, W.M. Zhao, R.X. Zhang, J. Chen, L. Zhou, Organocatalytic cycloaddition-elimination cascade for atroposelective construction of heterobiaryls, Chem. Sci. 12(44) (2021) 14920-14926. https://doi.org/10.1039/d1sc05161j.

[50] D. Villaseñor-Basulto, A. Picos-Benítez, N. Bravo-Yumi, T. Perez-Segura, E.R. Bandala, J.M. Peralta-Hernández, Electro-Fenton mineralization of diazo dye Black NT2 using a pre-pilot flow plant, J. Electroanal. Chem. 895 (2021) 115492. https://doi.org/10.1016/j.jelechem.2021.115492.

[51] M.A. Oturan, Outstanding performances of the BDD film anode in electro-Fenton process: Applications and comparative performance, Curr. Opin. Solid State Mater. Sci. 25(3) (2021) 100925. https://doi.org/10.1016/j.cossms.2021.100925.

[52] Y. Wang, M. Brigante, G. Mailhot, D. Talaga, Y. Wu, W. Dong, S. Sobanska, Toward a better understanding of ferric-oxalate complex photolysis: The role of the aqueous/air interface of droplet, Chemosphere 289 (2022) 133127. https://doi.org/10.1016/j.chemosphere.2021.133127.

[53] K. Hanna, S. Chiron, M.A. Oturan, Coupling enhanced water solubilization with cyclodextrin to indirect electrochemical treatment for pentachlorophenol contaminated soil remediation, Water Res. 39(12) (2005) 2763-2773. https://doi.org/10.1016/j.watres.2005.04.057.

[54] A. Ekpe, J.H. Tong, L. Rodriguez, High-performance liquid chromatographic method development and validation for the simultaneous quantitation of naproxen sodium and pseudoephedrine hydrochloride impurities, J. Chromatogr. Sci. 39(3) (2001) 81-6. https://doi.org/10.1093/chromsci/39.3.81.

[55] Y. Yang, Y. Xia, F. Wei, G. Teng, Y. Yao, Preparation and characterization of hydrophobic stearic acid-Yb-PbO_2 anode and its application on the electrochemical degradation of naproxen sodium, J. Electroanal. Chem. 868 (2020) 114191. https://doi.org/10.1016/j.jelechem.2020.114191.

[56] A. John, M.S. Rajan, J. Thomas, Carbon nitride-based photocatalysts for the mitigation of water pollution engendered by pharmaceutical compounds, Environ. Sci. Pollut. Res. 28(20) (2021) 24992-25013. https://doi.org/10.1007/s11356-021-13528-y.

[57] L. Xu, X. Ma, J. Niu, J. Chen, C. Zhou, Removal of trace naproxen from aqueous solution using a laboratory-scale reactive flow-through membrane electrode, J. Hazard. Mater. 379 (2019) 120692. https://doi.org/10.1016/j.jhazmat.2019.05.085.

[58] N.J. Bunce, L. Liu, J. Zhu, D.A. Lane, Reaction of Naphthalene and Its Derivatives with Hydroxyl Radicals in the Gas Phase, Environ. Sci. Technol. 31(8) (1997) 2252-2259. https://doi.org/10.1021/es960813g.

[59] E. Marco-Urrea, M. Pérez-Trujillo, P. Blánquez, T. Vicent, G. Caminal, Biodegradation of the analgesic naproxen by Trametes versicolor and identification of intermediates using HPLC-

DAD-MS and NMR, Bioresour. Technol. 101(7) (2010) 2159-2166. https://doi.org/10.1016/j.biortech.2009.11.019.

[60] R. Zhang, Y. Li, Z. Wang, Y. Tong, P. Sun, Biochar-activated peroxydisulfate as an effective process to eliminate pharmaceutical and metabolite in hydrolyzed urine, Water Res. 177 (2020) 115809. https://doi.org/10.1016/j.watres.2020.115809.

[61] O. Paltiel, G. Fedorova, G. Tadmor, G. Kleinstern, Y. Maor, B. Chefetz, Human Exposure to Wastewater-Derived Pharmaceuticals in Fresh Produce: A Randomized Controlled Trial Focusing on Carbamazepine, Environ. Sci. Technol. 50(8) (2016) 4476-82. https://doi.org/10.1021/acs.est.5b06256.

[62] S. Giannakis, I. Hendaoui, M. Jovic, D. Grandjean, L.F. De Alencastro, H. Girault, C. Pulgarin, Solar photo-Fenton and UV/H_2O_2 processes against the antidepressant Venlafaxine in urban wastewaters and human urine. Intermediates formation and biodegradability assessment, Chem. Eng. J. 308 (2017) 492-504. https://doi.org/10.1016/j.cej.2016.09.084.

[63] S. Giannakis, B. Androulaki, C. Comninellis, C. Pulgarin, Wastewater and urine treatment by UVC-based advanced oxidation processes: Implications from the interactions of bacteria, viruses, and chemical contaminants, Chem. Eng. J. 343 (2018) 270-282. https://doi.org/10.1016/j.cej.2018.03.019.

[64] S. Giannakis, S. Rtimi, C. Pulgarin, Light-Assisted Advanced Oxidation Processes for the Elimination of Chemical and Microbiological Pollution of Wastewaters in Developed and Developing Countries, Molecules 22(7) (2017). https://doi.org/10.3390/molecules22071070.

[65] G.V. Buxton, C.L. Greenstock, W.P. Helman, A.B. Ross, Critical Review of Rate Constants for Reactions of Hydrated Electrons, Hydrogen Atoms and Hydroxyl Radicals ($^{\bullet}OH/^{\bullet}O^{-}$) in Aqueous Solution, J. Phys. Chem. Ref. Data 17(2) (1988) 513-886. https://doi.org/10.1063/1.555805.

Supplementary Information

Electrochemical oxidation of Naproxen in aqueous matrices: Elucidating the intermediates' eco-toxicity, by assessing its degradation pathways via experimental and density functional theory approaches

Ling Feng[1], Weiwei Song[1], Nihal Oturan[2], Minoo Karbasi[3], Eric D. van Hullebusch[4], Giovanni Esposito[5], Stefanos Giannakis[6*], Mehmet A. Oturan[2*]

[1] School of Ecology and Environment, Inner Mongolia University, University W. Road, 010021, Huhhot, Inner Mongolia (P.R.), China

[2] Laboratoire Géomatériaux et Environnement (LGE), Université Paris-Est, EA 4508, 77454 Marne la Vallée, France

[3] Department of Materials Engineering, Bu-Ali Sina University, Hamedan 65178-38695, Iran

[4] Institut de Physique Du Globe de Paris, Université de Paris, CNRS, F-75005, Paris, France

[5] Department of Civil, Architectural and Environmental Engineering, University of Napoli "Federico II", Via Claudio 21, 80125 Napoli, Italy

[6] Universidad Politécnica de Madrid, E.T.S. de Ingenieros de Caminos, Canales y Puertos, Departamento de Ingeniería Civil: Hidráulica, Energía y Medio Ambiente, Unidad docente Ingeniería Sanitaria, c/ Profesor Aranguren, s/n, ES-28040 Madrid, Spain

**** Corresponding Author's E-mail: +***

stefanos.giannakis@epfl.ch (Stefanos Giannakis)

mehmet.oturan@univ-eiffel.fr (Mehmet A. Oturan)

There are 9 Pages with 4 Tables and 5 Figures in SI

Summary

Table S1. Basic physico-chemical information of naproxen.

Naproxen	Formula: $C_{14}H_{14}O_3$	Structure
Molecular weight (g mol^{-1}): 230.3	Solubility (at 20°C): 15.9 $mg \cdot L^{-1}$	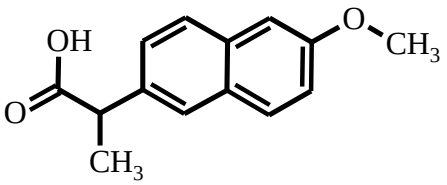
pKa (25°C): 4.15	Log Kow: 3.18	

Table S2. Basic information of intermediates products.

Intermediates	Formula	Molecular weight (g mol^{-1})	Log Kow	pKa (25°C)
Catechol	$C_6H_6O_2$	110	0.88	pK_{a1}: 9.45; pK_{a2}: 12.8
Phthalic acid	$C_8H_6O_4$	166	0.73	pK_{a1}: 2.76; pK_{a2}: 4.92
Hydroquinone	$C_6H_6O_2$	110	0.59	9.96
Benzoic acid	$C_7H_6O_2$	122	1.87	4.204
Phenol	C_6H_6	94	1.46	9.99
Phthalic anhydride	$C_8H_4O_3$	148	1.60	-
Pyrogallol	$C_6H_6O_3$	126	0.97	9.01
3-hydroxybenzoic acid	$C_7H_6O_3$	138	-	4.06
2-naphthol	$C_{10}H_8O$	144	2.70	9.51
1-naphthalene acetic acid	$C_{12}H_{10}O_2$	186	2.24	4.23
1,5-dihydroxynaphthalene	$C_{10}H_8O_2$	160	1.96	-
Glycolic	$C_2H_4O_3$	76.05	-1.11	3.83
Oxalic	$C_2H_2O_4$	90	-0.81	pK_{a1}: 1.46; PK_{a2}: 4.40
Formic	CH_2O_2	46	-0.54	3.75
Acetic	$C_2H_4O_2$	60	-0.17	4.76
Malic	$C_4H_6O_5$	134	-1.26	pK_{a1}: 3.51; pK_{a2}: 5.03
Glyoxylic	$C_2H_2O_3$	74	-0.07	3.30

Table S3. Apparent rate constants (min^{-1}) for oxidative degradation of naproxen at various current intensities by EAOPs.

mA	EF-Pt	EF-BDD	AO-BDD
	k_{app} = 0.113	k_{app} = 0.144	k_{app} =0.018
	(R^2 = 0.995)	(R^2 = 0.981)	(R^2 = 0.998)
	k_a = 0.100	k_a = 0.125	k_a = 0.018
0.10	α = 0.260	α = 0.238	α = 0.600
	(R^2 = 0.983)	(R^2 = 0.940)	(R^2 = 0.997)
	k_{app} = 0.170	k_{app} = 0.216	k_{app} = 0.029
	(R^2 = 0.990)	(R^2 = 0.988)	(R^2 = 0.999)
	k_a = 0.147	k_a = 0.185	k_a = 0.029
0.30	α = 0.310	α = 0.400	α = 2.900
	(R^2 = 0.969)	(R^2 = 0.961)	(R^2 = 0.996)
	k_{app} =0.342	k_{app} = 0.654	k_{app} = 0.092
	(R^2 = 0.990)	(R^2 = 0.998)	(R^2 = 0.998)
	k_a = 0.307	k_a = 0.637	k_a = 0.131
0.75	α = 1.150	α = 9.100	α = 1.460
	(R^2 = 0.970)	(R^2 = 0.996)	(R^2 = 0.966)

Table S4. Apparent rate constants (min^{-1}) for oxidative degradation of naproxen at various current intensities by EAOPs in urine and wastewater.

A	Matrices	EF-Pt	EF-BDD	AO-BDD
0.10	*Urine*	k_{app} = 0.047	k_{app} = 0.056	k_{app} =0.016
		(R^2 = 0.988)	(R^2 = 0.961)	(R^2 = 0.900)
	Wastewater	k_{app} = 0.059	k_{app} = 0.067	k_{app} =0.017
		(R^2 = 0.966)	(R^2 = 0.971)	(R^2 = 0.920)
0.30	*Urine*	k_{app} = 0.051	k_{app} = 0.062	k_{app} = 0.019
		(R^2 = 0.972)	(R^2 = 0.988)	(R^2 = 0.951)
	Wastewater	k_{app} = 0.075	k_{app} = 0.100	k_{app} =0.031

		($R^2 = 0.976$)	($R^2 = 0.936$)	($R^2 = 0.911$)
0.75	*Urine*	k_{app} =0.068	k_{app} = 0.085	k_{app} = 0.051
		($R^2 = 0.956$)	($R^2 = 0.973$)	($R^2 = 0.957$)
	Wastewater	k_{app} = 0.223	k_{app} = 0.476	k_{app} =0.080
		($R^2 = 0.9879$)	($R^2 = 0.959$)	($R^2 = 0.900$)

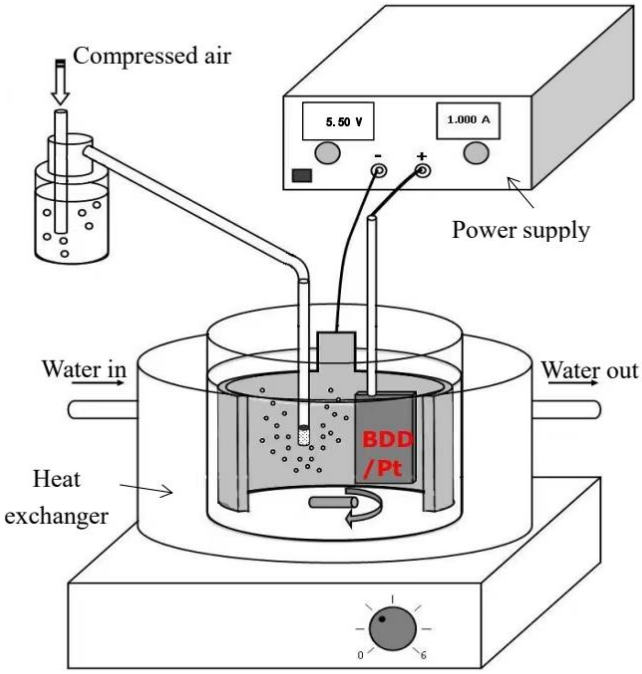

Fig. S1. Schematic diagram for EAOPs experiment set-up.

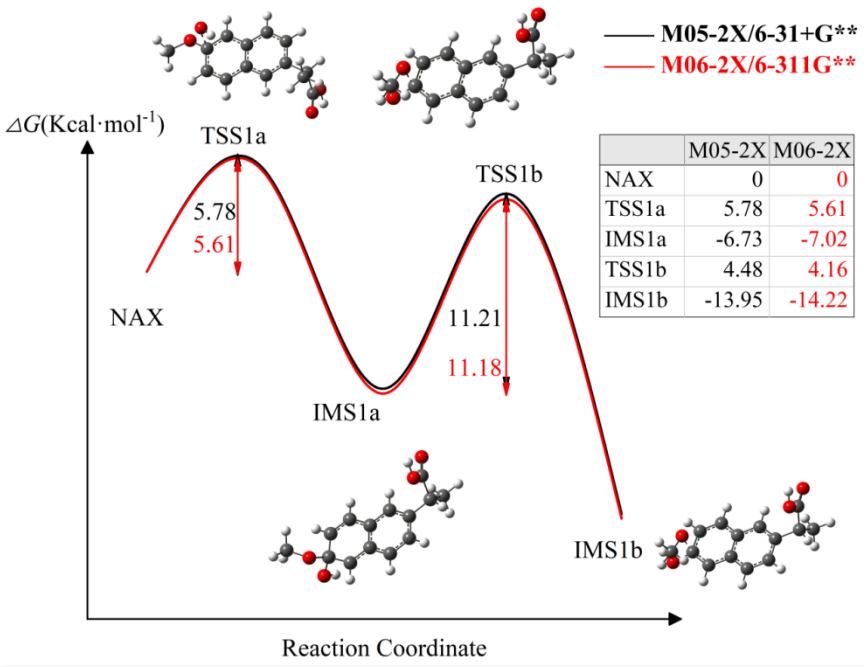

Fig. S2. △*G* for the formation of IMS1a to IMS1b in path A calculated by M06-2X/6-311g** and M05-2X/6-31+g**. This indicates that the results obtained by M05-2X and M06-2X are basically consistent.

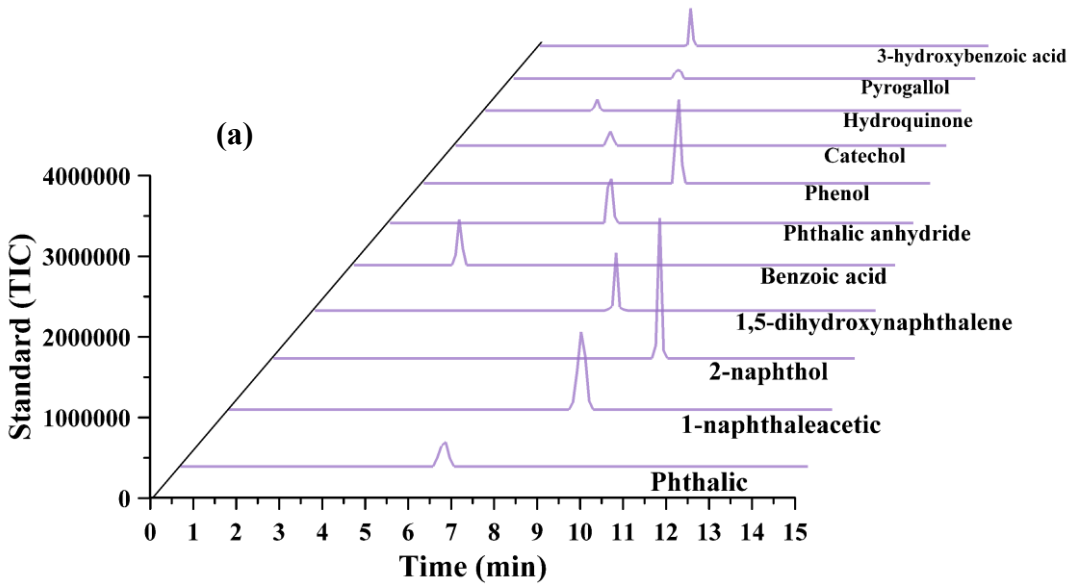

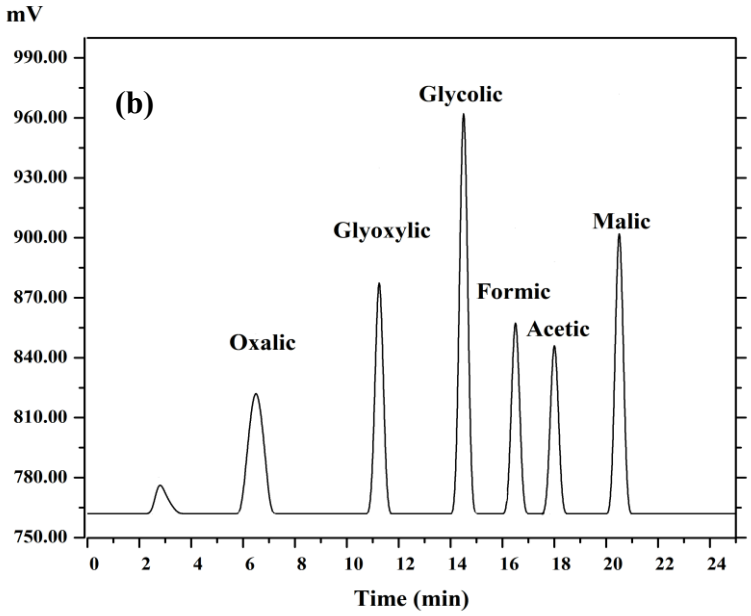

Fig. S3. Elution profiles for all the standard substances by HPLC. a: methanol/water/acetic acid (69:29:2 (v/v/v)) for aromatic intermediates; b: 1% H_3PO4 as eluent for short chain carboxylic acid.

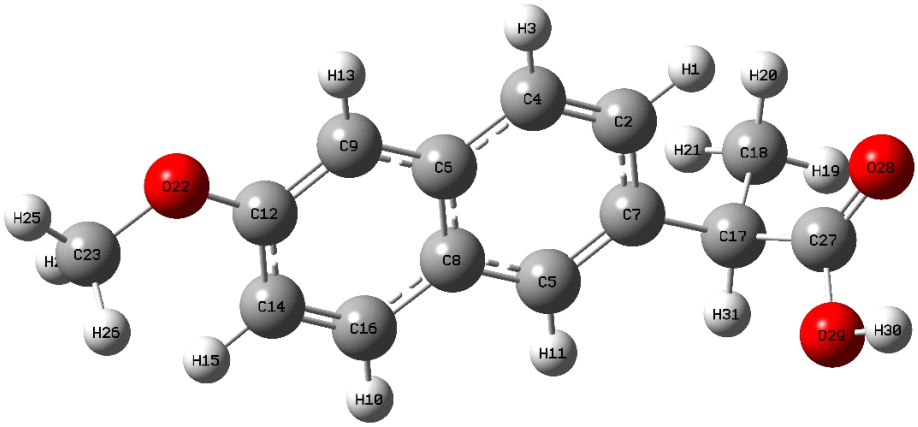

Fig. S4. Optimized structure of NAX under DFT.

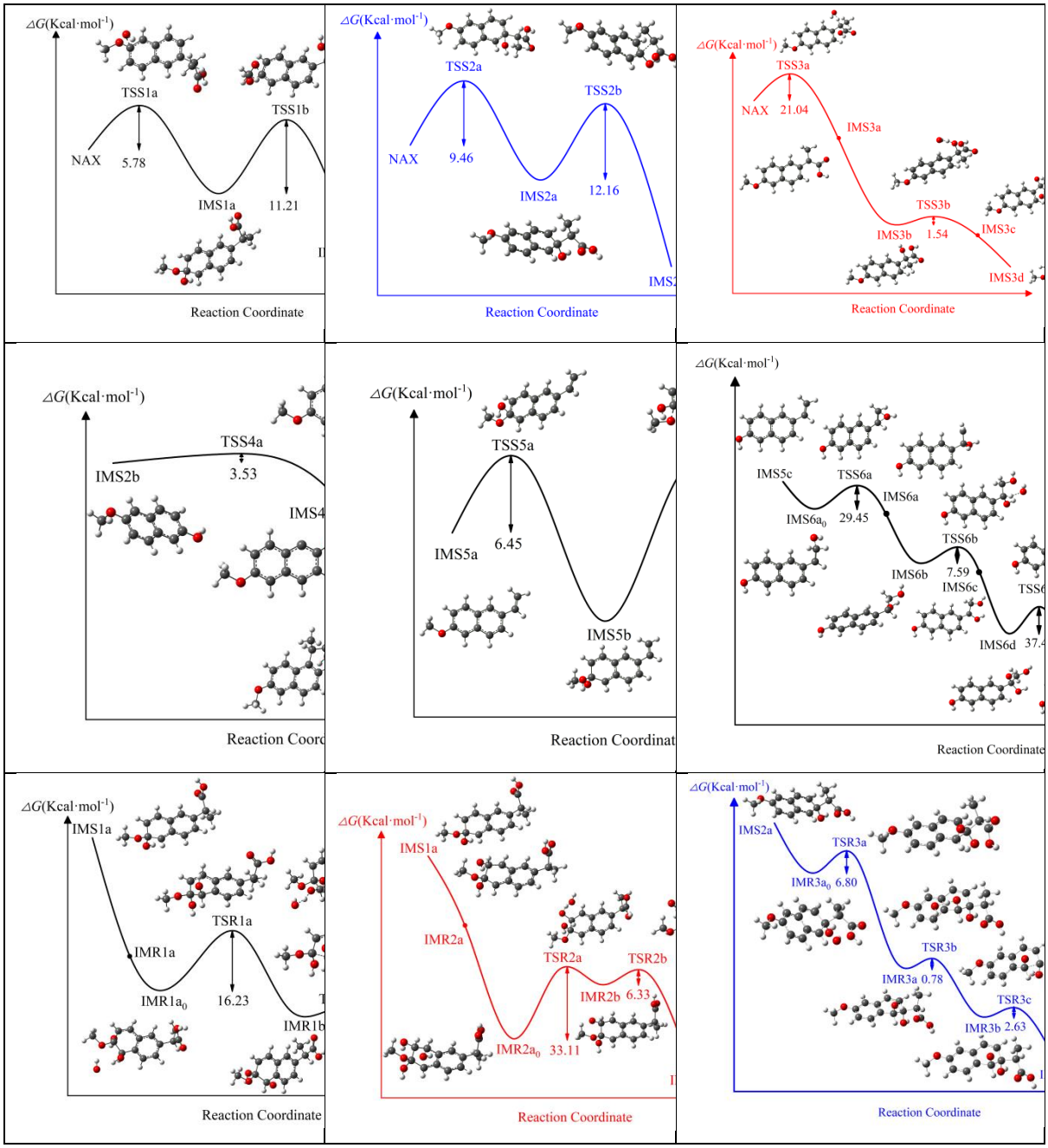

Fig. S5. Δ*G* for the formation of a-c: IMS1a to IMS3d for path A-C; d: IMS4a to IMS4b for path D; e: IMS5a to IMS5c for path E; f: IMS6c to IMS6f for path F; g-i: IMS1a to IMS3c path G-I.

APPENDIX A:

Imaginary Frequency and Cartesian Coordinates for Transition states

TSS1a in path A Imaginary Frequency: -165.45

H	2.03796000	2.63953900	-0.57242600
C	1.37088200	1.80914200	-0.37320500
H	-0.38882900	2.86685900	-0.98878500
C	0.01874100	1.93835100	-0.60698900
C	1.06078500	-0.46602400	0.38203200
C	-0.85574500	0.85670100	-0.35097100
C	1.90525800	0.60294400	0.12908500
C	-0.32186800	-0.36149400	0.14818000
C	-2.24895900	0.95776200	-0.58331300
H	-0.78707500	-2.39247500	0.75173800
H	1.45755900	-1.40244300	0.76184100
C	-3.09919700	-0.12711500	-0.30275700
H	-2.67575400	1.86146300	-0.99768000
C	-2.54832200	-1.36949600	0.16380900
H	-3.19560600	-2.21431300	0.34900700
C	-1.21005600	-1.46305200	0.38877200
C	3.39663500	0.48221100	0.39844800
C	3.70218600	0.23663600	1.87427900
H	3.31644000	1.06815400	2.46466600
H	4.77860100	0.16221100	2.03383300
H	3.23311100	-0.68484900	2.22066700
O	-4.36651100	-0.01264600	-0.73141700
C	-5.31911100	-0.99924300	-0.29587400
H	-5.12403600	-1.95544100	-0.77993600
H	-6.28802600	-0.61933200	-0.60514100
H	-5.28272800	-1.09870300	0.78881600
C	3.95008400	-0.62583700	-0.46819200
O	4.36142400	-1.69855900	-0.06595600
O	3.93163500	-0.30980600	-1.77138100
H	4.27453900	-1.05905600	-2.28668300
H	3.87622300	1.40378400	0.06248900
O	-3.36524200	0.99704400	1.54251200
H	-2.53069600	0.78741200	1.98770600

TSS1b in path A Imaginary Frequency: -465.10

H	-1.77565200	1.70283400	-2.15333300
C	-1.17368100	1.02409600	-1.56050200
H	0.68903700	1.72781300	-2.35229700
C	0.19961900	1.04037200	-1.67234400
C	-1.05173200	-0.74253300	0.08575900
C	0.99310900	0.16251400	-0.89488900
C	-1.81411500	0.12819000	-0.67794000
C	0.35051600	-0.74377600	-0.00526600
C	2.40320200	0.15812200	-0.99368700
H	0.65011500	-2.37018500	1.40629200
H	-1.53185300	-1.43956500	0.76618000
C	3.16276200	-0.66239600	-0.14372000
H	2.91031000	0.82233300	-1.68199800
C	2.50645000	-1.64678500	0.68083900
H	3.12216400	-2.33292300	1.25087900
C	1.15407800	-1.65724400	0.76416400
C	-3.33099100	0.10195000	-0.58831100
C	-3.91511500	-1.21147600	-1.10484900
H	-3.62859300	-1.34676900	-2.14814300
H	-5.00375700	-1.19909000	-1.03817600
H	-3.53818400	-2.05589600	-0.52664400
O	3.22524100	0.79607700	1.30165400
C	3.94614700	1.91174000	0.83544500
H	4.78521500	1.61175300	0.19625600
H	4.37175700	2.41896700	1.71063700
H	3.31543800	2.62585100	0.29503500
C	-3.73751500	0.35593800	0.84494000
O	-4.25604700	-0.45861800	1.58625000
O	-3.45306900	1.60497600	1.24303100
H	-3.71136600	1.71132300	2.17422100
H	-3.71792800	0.94071200	-1.17067200
O	4.48346200	-0.78798400	-0.42696500
H	4.91018800	-1.36504800	0.22216400

TSS2a in path B Imaginary Frequency: -161.74

H	-1.85029200	2.16121900	-0.86355900
C	-1.09445700	1.41846100	-0.64683400
H	0.50346800	2.81847400	-0.68024900
C	0.21176100	1.78285100	-0.54888600
C	-0.50430900	-0.91619300	-0.29135500
C	1.23744400	0.81024800	-0.29927200
C	-1.50258600	0.05030400	-0.46391900
C	0.86065800	-0.55542100	-0.18415100
C	2.58775000	1.16968800	-0.19024400
H	1.58165500	-2.56656000	0.12070700
H	-0.76245500	-1.96487000	-0.21866900

C	3.55261600	0.19697500	0.02874600
H	2.88729200	2.20744800	-0.27742300
C	3.19222300	-1.16571200	0.14091800
H	3.94066300	-1.92654000	0.30941300
C	1.86632900	-1.52437400	0.03407300
C	-2.93778900	-0.34039700	-0.80186000
C	-3.15335700	-1.83483100	-1.00399700
H	-2.50287800	-2.20095700	-1.79845700
H	-4.18800700	-2.01970000	-1.29133200
H	-2.94752800	-2.39491300	-0.09040700
O	4.83803600	0.63614400	0.12233000
C	5.87128800	-0.33566800	0.33020300
H	5.90263500	-1.04357900	-0.49886700
H	6.79755000	0.23021800	0.36823400
H	5.71874200	-0.86100800	1.27372800
C	-3.90393600	0.18729900	0.24214000
O	-4.62785800	-0.50868500	0.93053200
O	-3.94217700	1.52344000	0.30053700
H	-4.57439200	1.78751400	0.98971900
H	-3.18994700	0.19051800	-1.72594200
O	-1.66057100	-0.03816500	1.70793900
H	-1.87775600	-0.97853300	1.81902100

TSS2b in path B Imaginary Frequency: -560.08

H	1.80304800	2.88366100	0.21587100
C	1.12411400	2.06913700	-0.01065000
H	-0.57431200	2.97550900	0.87853200
C	-0.18043100	2.11332500	0.35282200
C	0.77100500	-0.09084600	-1.12805200
C	-1.07953700	1.03457400	0.03147800
C	1.67057400	0.89419100	-0.66813300
C	-0.57901400	-0.06958800	-0.72362200
C	-2.42408400	1.05930300	0.42131100
H	-1.10958900	-1.94849200	-1.64697200
H	1.14156100	-0.89472900	-1.75227000
C	-3.27552600	0.01901100	0.07594800
H	-2.80971400	1.89394900	0.99535400
C	-2.80021400	-1.07614400	-0.67925900
H	-3.45790400	-1.88860900	-0.95341400
C	-1.47860900	-1.10903500	-1.06931300
C	2.51056700	-0.01690400	1.04212000
C	1.40396300	-0.48349300	1.93523200
H	0.71764900	0.33383500	2.15964300
H	1.81691800	-0.83708500	2.88599300
H	0.84780400	-1.30473500	1.48301700
O	-4.56918200	0.12847100	0.50322600
C	-5.47613400	-0.92855400	0.16903200
H	-5.14238500	-1.87195900	0.60327200
H	-6.43051700	-0.64129100	0.60115200
H	-5.57348400	-1.02356800	-0.91336400
C	3.32331100	-1.04067900	0.41258300
O	2.93711800	-2.17142600	0.11098100
O	4.58805200	-0.64468500	0.13313600
H	5.03990700	-1.37011700	-0.32758300
H	3.07041500	0.85558900	1.36305400
O	2.81474300	1.05603600	-1.44358200
H	3.43484000	1.64509600	-0.99135100

TSS3a in path C Imaginary Frequency: -1194.41

H	1.77270800	-2.30450300	0.29618100
C	1.00986300	-1.53366700	0.26484700
H	-0.60297000	-2.91855800	0.08390100
C	-0.30891100	-1.87741600	0.14620500
C	0.45087000	0.81731000	0.29609100
C	-1.31871800	-0.87518700	0.10119400
C	1.40385800	-0.16667600	0.34362000
C	-0.92578800	0.48947800	0.17663200
C	-2.68770400	-1.20033400	-0.01784800
H	-1.63483400	2.52774200	0.18333200
H	0.74067500	1.86034500	0.34932900
C	-3.63928300	-0.20532600	-0.06250700
H	-2.99777900	-2.23674100	-0.07562800
C	-3.25779000	1.15858400	0.00995300
H	-4.00100600	1.94218300	-0.02619100
C	-1.92962300	1.48640400	0.12704800
C	2.87322500	0.14677300	0.49540600
C	3.47517100	-0.30275000	1.81436300
H	4.52502300	-0.01758600	1.87681600
H	3.40508200	-1.38886800	1.90617000
H	2.92889400	0.15192000	2.63984800
O	-4.93966200	-0.60997900	-0.17798500
C	-5.94853600	0.39933900	-0.23462200
H	-5.95644900	0.99649100	0.67869500
H	-6.89158300	-0.13221100	-0.32989800
H	-5.80502900	1.04712600	-1.10099000
C	3.65755700	-0.35384000	-0.69198900
O	4.57455600	-1.14691300	-0.62965500
O	3.22528900	0.17083200	-1.84470200
H	3.76336100	-0.19120500	-2.56798800
H	2.99246900	1.30878600	0.43966500
O	3.12122100	2.69203400	0.12960500
H	2.78507700	2.61112300	-0.78170100

TSS3b in path C Imaginary Frequency: -713.04

H	1.78931900	-2.21011400	0.03962100
C	1.00957100	-1.46029200	0.10068700
H	-0.55718600	-2.87915600	-0.23789300
C	-0.30832500	-1.84157900	-0.05527300
C	0.30871600	0.85330700	0.40375100
C	-1.36726400	-0.88160900	0.01885000
C	1.34070600	-0.11667600	0.31833700
C	-1.03778700	0.48211600	0.27287400
C	-2.69932600	-1.25537000	-0.12271000
H	-1.83241600	2.46515200	0.57100000
H	0.56629700	1.86773800	0.67064300
C	-3.71722200	-0.29113000	-0.01795700
H	-2.97620000	-2.28539200	-0.30876300
C	-3.40355200	1.05995000	0.23726600
H	-4.17934800	1.80616300	0.32183000
C	-2.08159000	1.42872200	0.37910800
C	2.77690400	0.34729100	0.53033300
C	3.10874900	0.20297100	2.01802400
H	4.13282000	0.53757400	2.18246800
H	3.00941900	-0.82999800	2.35289500
H	2.42702200	0.83664000	2.58621900
O	-4.96177400	-0.75187700	-0.17144800
C	-6.05954200	0.16731400	-0.07163200
H	-6.08262700	0.61967100	0.91955100
H	-6.95017700	-0.43107800	-0.22920400
H	-5.98116000	0.93289700	-0.84316300
C	3.72803200	-0.53476200	-0.29659000
O	4.66118300	-1.16996800	0.14240200
O	3.44288800	-0.48503900	-1.60575800
H	4.09851100	-1.01531900	-2.08454900
O	2.95790300	1.66314600	0.11661500
H	2.25244000	1.80350500	-0.77272900
O	1.30500300	1.83294100	-1.63292700
H	1.45324700	1.10657300	-2.24939100

TSS4a in path D Imaginary Frequency: -1217.60

H	2.85925300	-2.75927600	0.00077800
C	2.15410400	-1.93616700	-0.00050800
H	0.40938700	-3.16144100	0.00236900
C	0.80663800	-2.15373300	0.00040000
C	1.79116700	0.55167800	-0.00590200
C	-0.11394900	-1.04819100	-0.00070200
C	2.62716100	-0.59774500	-0.00207900
C	0.41325200	0.28679500	-0.00406100
C	-1.48289000	-1.26002000	0.00137400
H	-0.12784900	2.37536700	-0.00806100
H	2.35610800	1.86356800	-0.00889800
C	-2.36754100	-0.16451500	0.00053200
H	-1.89375900	-2.26269400	0.00376600
C	-1.88021000	1.15928800	-0.00328900
H	-2.55563400	2.00222100	-0.00417300
C	-0.51830900	1.36463400	-0.00559900
O	-3.67088400	-0.47911200	0.00382200
C	-4.63820800	0.58620800	0.00416400
H	-4.52165300	1.19663000	0.89923400
H	-4.52699400	1.19242700	-0.89442800
H	-5.60540100	0.09402200	0.00818100
O	3.94784300	-0.35375100	0.00045500
H	4.45970400	-1.17727700	0.00341900
O	2.80557700	2.96318300	-0.01803800
H	3.73925800	2.86449000	0.20192800

TSS5a in path E Imaginary Frequency: -148.92

H	-3.11678200	2.33186400	-0.27031700
C	-2.38372900	1.53483100	-0.22022000
H	-0.71073900	2.85199700	-0.45613100
C	-1.04302000	1.82896600	-0.32512100
C	-1.89400900	-0.81963600	0.02009500
C	-0.08055200	0.79505900	-0.25830900
C	-2.83518600	0.20271100	-0.04609600
C	-0.52189200	-0.54512900	-0.08496400
C	1.30544900	1.05969300	-0.35156000
H	0.10677700	-2.61518900	0.07619000
H	-2.20282300	-1.84942600	0.15689900
C	2.23897800	0.01168100	-0.26945000
H	1.66558900	2.06830400	-0.51111800
C	1.78893000	-1.34539600	-0.14181800
H	2.50384300	-2.15483600	-0.11094800
C	0.45660400	-1.59543800	-0.03575100
C	-4.28653800	-0.03018300	0.05615800
C	-4.89687200	-1.21671400	0.15081100
H	-5.97634200	-1.26909800	0.22118700
H	-4.35506800	-2.15547000	0.15967500
O	3.51312700	0.33166100	-0.54627700
C	4.53052700	-0.65386500	-0.29195000
H	4.44939300	-1.01626200	0.73274200
H	5.47383300	-0.13527500	-0.43306400
H	4.44860400	-1.47567400	-1.00214700
H	-4.89268700	0.87089500	0.04588800
O	2.19090000	0.63600800	1.85433700

H	2.70205200	1.44733900	1.71572000

TSS5b in path E Imaginary Frequency: -460.74

H	3.02147300	2.35660900	0.39664100
C	2.30611000	1.57224800	0.17804000
H	0.64022600	2.91103700	0.05939900
C	0.98116200	1.88482100	-0.00938000
C	1.84834100	-0.77486500	-0.19309500
C	0.03528800	0.86435600	-0.28829800
C	2.76592200	0.23248500	0.09557100
C	0.49087700	-0.48536100	-0.38683400
C	-1.32609500	1.15466500	-0.48789600
H	-0.08894900	-2.53277900	-0.83270300
H	2.16818600	-1.80690400	-0.27727700
C	-2.24711500	0.10029600	-0.64973600
H	-1.68502900	2.17617100	-0.44730800
C	-1.77371900	-1.24370800	-0.86346800
H	-2.49930700	-2.00880700	-1.10821900
C	-0.45602100	-1.52073400	-0.70903400
C	4.19875000	-0.01950300	0.31687700
C	4.80680100	-1.21179000	0.33221900
H	5.87366600	-1.27510700	0.50738700
H	4.27613900	-2.14415900	0.17776200
H	4.79449600	0.87250200	0.48712800
O	-2.46217600	-0.01296900	1.42430500
C	-3.73286700	-0.57824800	1.62117300
H	-4.54413700	0.08499500	1.30084400
H	-3.85104800	-0.74446000	2.70090200
H	-3.84316500	-1.54798900	1.11992300
O	-3.52355300	0.33196600	-1.04045300
H	-3.76133500	1.25894400	-0.89212700

TSS6a in path F Imaginary Frequency: -236.76

H	1.88722300	2.58343300	-0.14257200
C	1.22097600	1.72816600	-0.14653100
H	-0.54745600	2.90817300	0.06404600
C	-0.13282300	1.91137800	-0.03149300
C	0.93679900	-0.66999400	-0.27293700
C	-1.01495500	0.79712700	-0.03130500
C	1.77896000	0.42548200	-0.27943000
C	-0.46247100	-0.50995500	-0.15139400
C	-2.41898400	0.95614400	0.08988100
H	-0.92275300	-2.62465300	-0.23399900
H	1.33192100	-1.67667900	-0.34959300
C	-3.23144400	-0.15076600	0.09238800
H	-2.84362000	1.95006800	0.18183300
C	-2.69514400	-1.45882300	-0.02599700
H	-3.37306800	-2.30328700	-0.01946000
C	-1.34235800	-1.62939500	-0.14386500
C	3.23526500	0.30513800	-0.40422500
C	3.91040400	-0.80904800	-0.81597300
H	4.98192500	-0.77136600	-0.95646700
H	3.40563400	-1.74235300	-1.02722200
H	3.79186100	1.22769600	-0.28165600
O	-4.59610600	-0.07010300	0.20926700
H	-4.86796100	0.85398600	0.29370600
O	3.81085700	-0.61308000	1.50176700
H	4.73293300	-0.31228600	1.50839600

TSS6b in path F Imaginary Frequency: -773.78

H	-1.18445100	2.45540900	-0.24528200
C	-0.49797500	1.61929700	-0.18498600
H	1.24367900	2.85383100	-0.16320700
C	0.85263300	1.84324600	-0.13796500
C	-0.16013900	-0.77031700	-0.05793300
C	1.76514500	0.75520300	-0.04779700
C	-1.02342800	0.29693500	-0.14958000
C	1.24387200	-0.56642300	-0.00657500
C	3.16748600	0.95925100	0.00619700
H	1.75499200	-2.66652300	0.11280500
H	-0.52315700	-1.79105700	-0.02881100
C	4.00889800	-0.12256200	0.09773500
H	3.56837800	1.96680700	-0.02249200
C	3.50294700	-1.44571000	0.13536800
H	4.20182600	-2.26995700	0.20585900
C	2.15047300	-1.65775700	0.08369900
C	-2.51399000	0.13451700	-0.19923400
C	-3.03479800	-1.28810800	-0.20828600
H	-2.68753300	-1.82205800	0.67773200
H	-2.70179100	-1.80392700	-1.11237400
H	-2.93389500	0.60558300	0.76030800
O	5.37547800	-0.00060400	0.15931600
H	5.62861800	0.93198900	0.13177800
O	-3.02728700	0.87268000	-1.29124500
H	-3.98527700	0.73357300	-1.31371600
O	-4.46207000	-1.17864900	-0.19602200
H	-4.84489400	-2.06259900	-0.24301000
O	-4.09321800	0.82958000	1.81106900
H	-4.64646300	0.13943200	1.39161100

TSS6c in path F Imaginary Frequency: -1397.54

H	-1.28110500	-2.45508200	-0.10166100

C	-0.59537900	-1.61685800	-0.07976000
H	1.14828100	-2.84630700	-0.02176500
C	0.75557000	-1.83621600	-0.03794000
C	-0.25947500	0.77724300	-0.06947900
C	1.66789000	-0.74386300	-0.01877500
C	-1.11899300	-0.29462000	-0.08893900
C	1.14624400	0.57758900	-0.04020400
C	3.07099500	-0.94379100	0.02099300
H	1.65485900	2.68140600	-0.04351100
H	-0.62094100	1.79857400	-0.08309300
C	3.91227200	0.14200500	0.03948700
H	3.47281900	-1.95117400	0.03908600
C	3.40534500	1.46491400	0.01438600
H	4.10377200	2.29241600	0.02817800
C	2.05169900	1.67292700	-0.02523800
C	-2.61448400	-0.13529800	-0.16253600
C	-3.13040400	1.29024600	-0.09879800
H	-2.85306500	1.78651700	-1.03214500
H	-2.68553000	1.81789900	0.74561300
O	5.27956700	0.02347700	0.08381100
H	5.53326200	-0.90922300	0.10522200
O	-3.24499000	-0.95726800	-1.04160300
H	-3.62399700	-1.40403000	0.19170700
O	-4.54474800	1.22684100	0.04912800
H	-4.86141700	2.10616800	0.28639500
O	-3.21535300	-0.88180400	1.11783700
H	-3.93042500	-0.33280500	1.49339800

TSS6d in path F Imaginary Frequency: -485.63

H	-1.43111800	2.32828300	0.30603000
C	-0.71093700	1.52158700	0.24747400
H	0.97090500	2.82532500	0.07496700
C	0.62634700	1.79875700	0.11985600
C	-0.26586400	-0.85830900	0.23229200
C	1.58226500	0.74913700	0.04655300
C	-1.16297100	0.17823700	0.31047000
C	1.12309000	-0.59501900	0.10636500
C	2.97063900	1.01178300	-0.08498100
H	1.72644900	-2.67370400	0.07962600
H	-0.59992100	-1.88738500	0.26887100
C	3.85642900	-0.03488100	-0.15372400
H	3.32426600	2.03608100	-0.13254500
C	3.41216700	-1.37962300	-0.09387600
H	4.14521500	-2.17471500	-0.15155600
C	2.07517800	-1.64857500	0.03333700
C	-2.65845900	-0.07636500	0.40576000
C	-3.24495300	0.19978900	-1.10704100
H	-2.60918400	-0.43620300	-1.72424300
H	-3.11414600	1.25425900	-1.32842800
O	5.21163300	0.14542800	-0.28416600
H	5.41718700	1.08920600	-0.32475500
O	-3.32586200	0.79647300	1.14058800
O	-4.59588600	-0.13439900	-1.21101800
H	-4.68174100	-1.09379000	-1.28458700
O	-2.90512000	-1.42687400	0.71746200
H	-3.84362200	-1.51149800	0.93877700

TSR1a in path G Imaginary Frequency: -2111.18

H	2.30438500	1.98542200	1.83713100
C	1.70217700	1.28900100	1.26613200
H	-0.15173100	2.28099800	1.72815000
C	0.31824000	1.45356500	1.20923400
C	1.52735000	-0.65818900	-0.14298800
C	-0.46194500	0.55655000	0.49168000
C	2.31616600	0.23284200	0.59174100
C	0.14272900	-0.50645600	-0.19843100
C	-1.95159200	0.76788200	0.33836000
H	-0.20697900	-2.12907000	-1.63505400
H	1.99053700	-1.47863900	-0.67949300
C	-2.68393900	-0.57966700	0.22488000
H	-2.35529900	1.30711700	1.20180200
C	-2.02289600	-1.48773800	-0.78323800
H	-2.63433300	-2.19803300	-1.32337100
C	-0.69851300	-1.44794400	-0.94988000
C	3.82540100	0.05613900	0.67223100
C	4.22037200	-1.29042900	1.29026200
H	3.81376700	-2.12127200	0.71522100
H	5.30564200	-1.39246800	1.32779200
H	3.82886800	-1.34330500	2.30624600
O	-4.02468000	-0.27394000	-0.09013000
C	-4.90683300	-1.39139800	-0.27490900
H	-5.91142200	-1.01614100	-0.09945600
H	-4.83379800	-1.77138800	-1.29371000
H	-4.67798900	-2.17682000	0.44415800
C	4.40830600	0.26202800	-0.71074500
O	4.81193900	1.32509600	-1.13267800
O	4.41160900	-0.85291100	-1.45515700
H	4.75904000	-0.63423900	-2.33389700
H	4.22704600	0.87076700	1.27431000
O	-2.61460600	-1.23919700	1.47309400
H	-3.04545400	-0.68274900	2.13705400
O	-2.07119100	1.55600700	-0.83255200

H	-2.94855700	2.19878000	-0.76670500
O	-4.18101600	2.39177700	-0.76924600
H	-4.53029700	1.50927100	-0.53279600

TSR1b in path G Imaginary Frequency: -166.33

H	2.12606200	2.22975300	1.55460900
C	1.49025500	1.53618200	1.01672500
H	-0.26039600	2.78004800	1.17411300
C	0.14449500	1.84454500	0.80467100
C	1.18986900	-0.54277800	-0.15813700
C	-0.67726500	0.96917400	0.10469100
C	2.02149500	0.34316900	0.53257400
C	-0.15813900	-0.24966900	-0.36753400
C	-2.08496000	1.42147800	-0.19577600
H	-0.54718900	-1.89655500	-1.75737400
H	1.58685500	-1.48234000	-0.53074200
C	-3.04514800	-0.39462300	0.07999500
H	-2.64175800	1.82318600	0.66299500
C	-2.35058100	-1.25024100	-0.89586500
H	-2.98236900	-1.88855100	-1.50554200
C	-1.02195100	-1.21141900	-1.06423300
C	3.47972600	-0.01002900	0.77233800
C	3.63728100	-1.21430200	1.69808400
H	3.15960800	-2.09727700	1.27138700
H	4.69243800	-1.43418000	1.86478600
H	3.16889300	-0.99340700	2.65757200
O	-4.32673700	-0.04477100	-0.21365900
C	-5.33687500	-0.98239700	0.24822900
H	-6.26449800	-0.65897200	-0.21372600
H	-5.07986100	-1.98968200	-0.08054100
H	-5.42029000	-0.94153300	1.33260200
C	4.15150800	-0.25200100	-0.56004200
O	4.60173500	-1.31731800	-0.93984300
O	4.20046000	0.85439400	-1.31665200
H	4.62368300	0.64232400	-2.16570000
H	3.96884200	0.86461900	1.20667600
O	-2.77993300	-0.67146700	1.38408600
H	-3.27089800	-0.06568500	1.96357900
O	-2.38269800	1.81237700	-1.35506000

TSR2a in path H Imaginary Frequency: -343.48

H	-2.57154200	-2.57774000	1.09291500
C	-1.84129300	-1.83393500	0.79672700
H	-0.18021300	-3.16437400	1.01799100
C	-0.50901700	-2.16666000	0.75606300
C	-1.37603100	0.42520100	0.07075400
C	0.46235900	-1.19816500	0.37211000
C	-2.29539100	-0.53243700	0.45654000
C	-0.00056300	0.12080000	0.01893400
C	1.80870000	-1.50807000	0.31990200
H	0.55294900	2.00318100	-0.83309600
H	-1.69810000	1.42381100	-0.20706300
C	2.87659700	-0.49041900	0.03957400
H	2.14894600	-2.50612500	0.57140000
C	2.36014000	0.76113700	-0.72236900
H	2.31197800	0.44458300	-1.78316400
C	0.92471200	1.07455400	-0.41914200
C	-3.77380400	-0.19904800	0.51625800
C	-4.07781500	0.89874500	1.53359800
H	-3.75013300	0.57500600	2.52162300
H	-5.14943200	1.09714000	1.56593400
H	-3.55858100	1.82290000	1.27714200
O	3.85335500	-1.19677200	-0.69503900
C	4.96863100	-0.43146200	-1.17512700
H	4.66093100	0.24121700	-1.97614500
H	5.67865500	-1.15878200	-1.56177000
H	5.42610400	0.13602300	-0.36537700
C	-4.24126800	0.18715900	-0.87104400
O	-4.67733100	1.27690100	-1.18910300
O	-4.11942900	-0.82198100	-1.74483400
H	-4.41682700	-0.52501400	-2.62114600
H	-4.31487100	-1.11180900	0.77494200
O	3.40251000	-0.04874800	1.27601000
H	3.69033300	-0.82798700	1.77362700
O	3.14245200	1.89263300	-0.54018600
H	2.44317700	2.33255300	0.51252300
O	1.63469700	2.39339500	1.26851100
H	1.12085300	3.18759400	1.08011500

TSR2b in path H Imaginary Frequency: -775.56

H	2.27564100	2.63223500	-1.04523900
C	1.57239700	1.85294800	-0.77572900
H	-0.14605100	2.97353100	-1.33736500
C	0.24412600	2.03996300	-0.94974300
C	1.26498400	-0.40331200	0.09605200
C	-0.69486700	1.02128100	-0.53362600
C	2.09776400	0.62371500	-0.19892900
C	-0.15617200	-0.30426300	-0.18273100
C	-2.02914600	1.28773600	-0.44330200
H	-0.58653400	-2.36951300	0.08156900
H	1.63317100	-1.34630800	0.48721200
C	-2.98234600	0.39138900	0.20600500

H	-2.43928400	2.18960300	-0.88839900
C	-2.36109500	-1.35997800	-0.73983300
H	-2.46741500	-0.88610600	-1.72844000
C	-0.96581400	-1.39445700	-0.20696600
C	3.58856900	0.58868600	0.08085700
C	3.89979500	1.26646700	1.41669900
H	3.53362200	2.29363500	1.39598900
H	4.97527900	1.28240200	1.59758600
H	3.40856000	0.73656200	2.23361200
O	-4.25883500	0.59141000	-0.18559100
C	-5.31297100	0.02987400	0.62507800
H	-5.13753600	-1.03081700	0.79034400
H	-6.22053300	0.17846700	0.04802000
H	-5.37698200	0.56122600	1.57277300
C	4.10953200	-0.82723900	0.04725400
O	4.45524400	-1.47399100	1.01861200
O	4.15591300	-1.32536800	-1.19631500
H	4.48302600	-2.23990800	-1.16170500
H	4.09261400	1.12063100	-0.72994400
O	-2.87269300	0.07202900	1.53045500
H	-1.94186500	0.02100600	1.79474300
O	-3.19641100	-2.23826800	-0.38681800

TSR3a in path I Imaginary Frequency: -127.66

H	1.54817100	3.01979700	0.16160400
C	0.89765900	2.16446200	0.01605000
H	-0.85074500	3.12347200	0.71009700
C	-0.40361300	2.21974200	0.31434800
C	0.61414000	-0.21048000	-0.76639000
C	-1.27649700	1.07297500	0.09137300
C	1.56760800	0.93044700	-0.52889200
C	-0.72937900	-0.11912500	-0.49986300
C	-2.61752800	1.12403600	0.37837100
H	-1.16346600	-2.10080400	-1.24936000
H	1.00320600	-1.05999200	-1.30557800
C	-3.44344600	0.01165700	0.09592000
H	-3.06822800	2.00654000	0.81449100
C	-2.92897800	-1.16551700	-0.50648300
H	-3.57209600	-2.00424400	-0.72700400
C	-1.59362500	-1.21515200	-0.79801200
C	2.73317800	0.56401600	0.43393300
C	2.34222300	0.63951800	1.91075900
H	2.14314200	1.67119600	2.19471700
H	3.16063900	0.26834200	2.52434900
H	1.45382900	0.04004200	2.11183100
O	-4.71754700	0.15833100	0.42368000
C	-5.64688400	-0.91911200	0.17465700
H	-5.34438900	-1.80282500	0.73411000
H	-6.60299900	-0.55245900	0.53218200
H	-5.69357800	-1.12619300	-0.89303400
C	3.45244300	-0.73649100	0.12728300
O	4.09577200	-1.35374500	0.95841300
O	3.43320000	-1.10395400	-1.15615600
H	3.95444600	-1.91923100	-1.24949900
H	3.48602800	1.33677100	0.23245400
O	2.15561700	1.24703100	-1.79876100
H	1.47738900	1.65253000	-2.35725500
O	1.08301700	-2.24106600	0.79350800
H	1.86438000	-2.37159000	1.34210200

TSR3b in path I Imaginary Frequency: -1328.67

H	-1.69376000	-2.59748800	1.20545000
C	-1.00682700	-1.84910900	0.81979900
H	0.71153100	-2.79840800	1.61037400
C	0.31264900	-1.96007800	1.04704000
C	-0.71126500	0.53247200	0.08082700
C	1.26090800	-1.00060200	0.49074600
C	-1.57134900	-0.74073200	-0.04490100
C	0.75099100	0.20122700	-0.10456100
C	2.61722300	-1.24739900	0.45455600
H	1.24120200	1.98853300	-1.21267400
H	-1.04213500	1.24107800	-0.68809300
C	3.49568200	-0.33185500	-0.18716000
H	3.03815000	-2.15191100	0.88013600
C	2.99915900	0.83832500	-0.80582400
H	3.66196400	1.52351600	-1.31659000
C	1.64539600	1.10453000	-0.73555500
C	-3.08850700	-0.56516800	0.23533000
C	-3.46073800	-0.13038200	1.66283000
H	-2.98916600	-0.79356100	2.39259800
H	-4.54478300	-0.19270100	1.79679300
H	-3.12370400	0.88583900	1.85994800
O	4.78052200	-0.68295200	-0.17184400
C	5.76868300	0.16329100	-0.79651200
H	5.77274300	1.14903400	-0.32568700
H	6.71922600	-0.33823900	-0.62915100
H	5.56975700	0.24759300	-1.86748400
C	-3.70635300	0.38399000	-0.77464600
O	-3.49231200	1.58125300	-0.84144900
O	-4.56799800	-0.23936300	-1.60566500
H	-4.93928100	0.42509300	-2.21362400
H	-3.52827500	-1.55161800	0.05207000

O	-1.41877100	-1.09644600	-1.44347300
H	-1.73099000	-2.00356400	-1.57469100
O	-0.77588400	1.08490500	1.37284000
H	-0.01518900	1.89436900	1.41314800
O	1.01195700	2.74206600	1.39159600
H	0.75867300	3.56565900	0.94962500

TSR3c in path I Imaginary Frequency: -227.69

H	1.59144800	2.76803600	-0.47940600
C	0.93088700	1.91403000	-0.36516000
H	-0.80141500	3.08609200	-0.17301400
C	-0.38123900	2.08692900	-0.16456900
C	0.60861800	-0.46257100	0.96953900
C	-1.30305900	0.96293100	0.05147100
C	1.56195900	0.57383200	-0.46749900
C	-0.81189300	-0.27875200	0.49444200
C	-2.65580400	1.10741500	-0.23598700
H	-1.30577000	-2.31499500	0.93446100
H	1.07977600	-1.40123100	0.65220100
C	-3.52557300	0.01855900	-0.10860700
H	-3.04583400	2.05809800	-0.58047200
C	-3.04220800	-1.22254900	0.30245700
H	-3.69416200	-2.07860500	0.40052400
C	-1.68186600	-1.35436300	0.60044900
C	3.06235200	0.53278100	-0.23043900
C	3.54181300	1.16632500	1.07551100
H	3.10517000	2.15736300	1.19909800
H	4.62638300	1.27329400	1.03846200
H	3.27230300	0.55376200	1.93135400
O	-4.83276000	0.26464100	-0.41878600
C	-5.75241800	-0.82725800	-0.30811800
H	-5.79144700	-1.19190300	0.71932700
H	-6.72009500	-0.42562200	-0.59487400
H	-5.47035000	-1.63498700	-0.98520400
C	3.57946500	-0.88612300	-0.34604400
O	3.53480700	-1.70717600	0.55109300
O	4.11761100	-1.15509500	-1.53916100
H	4.43171600	-2.07569200	-1.54545200
H	3.47448000	1.09559200	-1.07509300
O	1.24914600	-0.17848400	-1.57236000
H	0.37383400	0.05939100	-1.91373300
O	0.94216500	0.03665000	2.08760700

APPENDIX B:

Spin Population and bond order analysis

Table B1 Spin Population of IMR1c

Atomic space	Value	% of sum	% of sum abs
1(H)	0.00023210	0.023210	0.018802
2(C)	0.09980876	9.980791	8.085473
3(H)	0.00029786	0.029785	0.024129
4(C)	-0.02325119	-2.325099	-1.883571
5(C)	0.09421964	9.421884	7.632700
6(C)	0.08208599	8.208529	6.649757
7(C)	-0.01743876	-1.743861	-1.412708
8(C)	-0.02359722	-2.359702	-1.911603
9(C)	0.04262411	4.262375	3.452965
10(H)	-0.00052863	-0.052862	-0.042824
11(H)	-0.00071265	-0.071265	-0.057732
12(C)	0.26254912	26.254690	21.269014
13(H)	0.00008137	0.008137	0.006592
14(C)	-0.05074991	-5.074948	-4.111232
15(H)	0.00179187	0.179185	0.145159
16(C)	0.37981225	37.980904	30.768459
17(C)	0.00029931	0.029931	0.024247
18(C)	-0.00081140	-0.081140	-0.065731
19(H)	0.00015476	0.015476	0.012537
20(H)	0.00007393	0.007393	0.005989
21(H)	0.00002207	0.002207	0.001788
22(O)	0.05548934	5.548887	4.495173
23(C)	0.00863494	0.863487	0.699514
24(H)	0.00011845	0.011845	0.009595
25(H)	0.00224841	0.224839	0.182143
26(H)	0.00018910	0.018910	0.015319
27(C)	-0.00002464	-0.002464	-0.001996
28(O)	0.00026085	0.026085	0.021131
29(O)	0.00037517	0.037517	0.030392
30(H)	-0.00000104	-0.000104	-0.000084
31(H)	-0.00009071	-0.009071	-0.007349
32(O)	0.04543744	4.543706	3.680871
33(H)	0.00284441	0.284439	0.230425
34(O)	0.03756336	3.756304	3.042995
Summing up above values:			1.00000845
Summing up absolute value of above values:			1.23442076

Table B2 Spin Population of IMR2c

Atomic space	Value	% of sum	% of sum abs
1(H)	-0.00038054	-0.038054	-0.028893
2(C)	0.13175471	13.175501	10.003437
3(H)	0.00007747	0.007747	0.005882
4(C)	-0.05690034	-5.690047	-4.320141
5(C)	0.11602233	11.602259	8.808960
6(C)	0.12611315	12.611343	9.575103
7(C)	-0.04668104	-4.668115	-3.544244
8(C)	-0.04048969	-4.048978	-3.074167
9(C)	-0.00356404	-0.356404	-0.270598
10(H)	-0.00308173	-0.308174	-0.233980
11(H)	-0.00137674	-0.137675	-0.104529
12(C)	0.05433020	5.433032	4.125004
13(H)	0.00205749	0.205750	0.156215
14(C)	0.03416844	3.416852	2.594229
15(H)	-0.00138423	-0.138424	-0.105098
16(C)	0.46048664	46.048767	34.962310
17(C)	0.00021875	0.021875	0.016609
18(C)	-0.00200987	-0.200988	-0.152599
19(H)	0.00004127	0.004127	0.003133
20(H)	-0.00053163	-0.053163	-0.040364
21(H)	0.00014243	0.014243	0.010814
22(O)	0.01500920	1.500923	1.139569
23(C)	0.00069274	0.069274	0.052596
24(H)	0.00020692	0.020692	0.015711
25(H)	-0.00003573	-0.003573	-0.002713
26(H)	0.00063533	0.063533	0.048237
27(C)	-0.00142595	-0.142596	-0.108265
28(O)	-0.00016329	-0.016329	-0.012398
29(O)	-0.00042117	-0.042117	-0.031977
30(H)	0.00001427	0.001427	0.001083
31(H)	-0.00010233	-0.010233	-0.007769
32(O)	0.01032078	1.032080	0.783602
33(H)	0.00039458	0.039458	0.029959
34(O)	0.20585940	20.585986	15.629813
Summing up above values:			0.99999776
Summing up absolute value of above values:			1.31709443

Table B3 Spin Population of IMR3c

Atomic space	Value	% of sum	% of sum abs
1(H)	0.00291143	0.291145	0.251353
2(C)	-0.05945768	-5.945798	-5.133161
3(H)	-0.00076349	-0.076349	-0.065914
4(C)	0.38523003	38.523202	33.258071
5(C)	0.02369624	2.369636	2.045768
6(C)	-0.01266077	-1.266083	-1.093042
7(C)	0.30665966	30.666125	26.474854
8(C)	0.04474334	4.474357	3.862827
9(C)	0.10090255	10.090307	8.711222
10(H)	0.00034303	0.034304	0.029615
11(H)	-0.00010274	-0.010274	-0.008870
12(C)	0.00035173	0.035173	0.030366
13(H)	-0.00040062	-0.040063	-0.034587
14(C)	0.05460690	5.460719	4.714379
15(H)	-0.00000091	-0.000091	-0.000078
16(C)	-0.00570515	-0.570518	-0.492543
17(C)	0.00404732	0.404734	0.349418
18(C)	0.00732719	0.732722	0.632578
19(H)	0.00002829	0.002829	0.002443
20(H)	0.00067345	0.067345	0.058141
21(H)	-0.00006393	-0.006393	-0.005520
22(O)	0.00415595	0.415597	0.358796
23(C)	0.00024046	0.024046	0.020759
24(H)	0.00020199	0.020199	0.017438
25(H)	0.00001299	0.001299	0.001122
26(H)	0.00024817	0.024817	0.021425
27(C)	0.01753482	1.753491	1.513834
28(O)	0.01222068	1.222074	1.055048
29(O)	0.00187629	0.187630	0.161986
30(H)	0.00068724	0.068724	0.059331
31(H)	0.00456733	0.456735	0.394311
32(O)	0.07626308	7.626347	6.584022
33(H)	0.00125067	0.125067	0.107974
34(O)	0.02836928	2.836943	2.449206
Summing up above values:			0.99999483
Summing up absolute value of above values:			1.15830539

Table B4 Bond Order Analysis of IMR1c, IMR2c and IMR3c

Bond order from mixed alpha&beta density matrix >= 0.050000								
	IMR1c			IMR2c			IMR3c	
#1	1(H)	2(C)						
	0.93111302		1(H)	2(C)	0.92847089	1(H)	2(C)	0.92466626
#2	2(C)	4(C)						
	1.43486614		2(C)	4(C)	1.44204066	2(C)	4(C)	1.37463083
#3	2(C)	7(C)						
	1.39155912		2(C)	7(C)	1.37486443	2(C)	7(C)	1.44055349
#4	2(C)	8(C)						
	0.06171618		2(C)	8(C)	0.05380271	3(H)	4(C)	0.93050747
#5	3(H)	4(C)						
	0.92643878		3(H)	4(C)	0.93040371	4(C)	6(C)	1.14910593
#6	4(C)	5(C)						
	0.07359912		4(C)	5(C)	0.07461763	5(C)	8(C)	1.03431014
#7	4(C)	6(C)						
	1.36410283		4(C)	6(C)	1.38728905	5(C)	11(H)	0.90998931
#8	5(C)	7(C)						
	1.44831510		5(C)	7(C)	1.47777894	5(C)	34(O)	1.79130677
#9	5(C)	8(C)						
	1.32846489		5(C)	8(C)	1.28498367	6(C)	8(C)	1.23782298
#10	5(C)	11(H)						
	0.91931451		5(C)	11(H)	0.91718935	6(C)	9(C)	1.37145292
#11	6(C)	7(C)						
	0.06326934		6(C)	7(C)	0.06519522	6(C)	14(C)	0.05310685
#12	6(C)	8(C)						
	1.30310129		6(C)	8(C)	1.30345030	7(C)	17(C)	0.98689011
#13	6(C)	9(C)						
	1.02272287		6(C)	9(C)	1.07159244	7(C)	32(O)	1.03082539
#14	7(C)	17(C)		7(C)	17(C)			
	0.97051545			0.96875824		8(C)	12(C)	0.05217443
#15	8(C)	16(C)		8(C)	16(C)			
	1.19967570			1.19375099		8(C)	16(C)	1.32380928
#16	9(C)	13(H)		9(C)	12(C)			
	0.91985562			1.63932062		9(C)	12(C)	1.36554123
#17	9(C)	34(O)		9(C)	13(H)			
	1.76299401			0.91642228		9(C)	13(H)	0.92992444
#18	10(H)	16(C)		10(H)	16(C)			
	0.92698433			0.92415024		9(C)	16(C)	0.06703778
#19	12(C)	14(C)		12(C)	22(O)			
	1.45737760			1.00173349		10(H)	16(C)	0.93098393
#20	12(C)	22(O)		12(C)	32(O)			
	1.00975515			1.02266659		12(C)	14(C)	1.31167668
#21	12(C)	32(O)		14(C)	15(H)	12(C)	22(O)	0.95971780

	1.02162711	0.91890713			
#22	14(C) 15(H)	14(C) 16(C)			
	0.92803485	1.15366053	14(C)	15(H)	0.92865297
#23	14(C) 16(C)	14(C) 34(O)			
	1.34405378	1.64642730	14(C)	16(C)	1.44932284
#24	17(C) 18(C)	17(C) 18(C)			
	0.99185015	0.99266111	17(C)	18(C)	0.99867096
#25	17(C) 27(C)	17(C) 27(C)			
	0.94749035	0.94765958	17(C)	27(C)	0.91421313
#26	17(C) 31(H)	17(C) 31(H)			
	0.91572976	0.91607754	17(C)	31(H)	0.92066407
#27	18(C) 19(H)	18(C) 19(H)			
	0.95422084	0.95509518	18(C)	19(H)	0.95610148
#28	18(C) 20(H)	18(C) 20(H)			
	0.95561459	0.95555710	18(C)	20(H)	0.95669257
#29	18(C) 21(H)	18(C) 21(H)			
	0.95479869	0.95405599	18(C)	21(H)	0.94818417
#30	22(O) 23(C)	22(O) 23(C)			
	0.82099296	0.82520527	22(O)	23(C)	0.87863503
#31	23(C) 24(H)	23(C) 24(H)			
	0.95682534	0.95083144	23(C)	24(H)	0.94442867
#32	23(C) 25(H)	23(C) 25(H)			
	0.94643245	0.95944482	23(C)	25(H)	0.96184898
#33	23(C) 26(H)	23(C) 26(H)			
	0.94620191	0.95025835	23(C)	26(H)	0.94436511
#34	27(C) 28(O)	27(C) 28(O)			
	1.79600650	1.79819428	27(C)	28(O)	1.83952269
#35	27(C) 29(O)	27(C) 29(O)			
	1.09274576	1.09155085	27(C)	29(O)	1.08435107
#36	29(O) 30(H)	29(O) 30(H)			
	0.81488069	0.81480926	28(O)	29(O)	0.06479980
#37	16(O) 17(H)	32(O) 33(H)			
	0.80751753	0.80931053	29(O)	30(H)	0.83943786
			32(O)	33(H)	0.80967069